INSTITUTE OF PLASMA PHYSICS
CZECHOSLOVAK ACADEMY OF SCIENCES

HARD X-RAY STUDIES ON THE CASTOR TOKAMAK

Jan Mlynář

RESEARCH REPORT

IPPCZ 299

April 1990

POD VODÁRENSKOU VĚŽÍ 4, 180 69 PRAGUE 8
CZECHOSLOVAKIA

HARD X-RAY STUDIES ON THE CASTOR TOKAMAK

Jan Mlynář *

Institute of Plasma Physics
Czechoslovak Academy of Science
Pod vodárenskou věží 4
182 11 Praha 8

* undergraduate student
Charles University
Faculty of Mathematics and Physics
Ke Karlovu 3
121 16 Praha 2

IPPCZ 299 April 1990

ABSTRACT

This report forms the basis for quantitative measurements of hard X-ray radiation. It deals with chosen general facts that must be taken into account before starting the experiments. Apart from this, first qualitative results of hard X-ray measurements on the Castor tokamak are presented. Performed were a series of integral measuremens which mapped the azimutal dependance of the radiation.

Introduction

High energy electrons, called runaway electrons are created in tokamak plasma by acceleration in an electric field. Distortion of the Maxwellian distribution is possible thanks to the quickly falling Coulombic momentum transfer cross-section with the energy of electrons in fully ionized plasma. Runaway electrons directly take part in some important processes (conduction of current, instabilities, energetic distribution...). The most direct method of their observation is the measurement of hard X-ray radiation.

Most of the hard X-rays are produced when the energetic electrons hit the limiter or the liner. However, some small fraction of the hard X-ray emission is produced in electron-ion collisions in the plasma. By careful experimentation the resulting plasma bremsstrahlung can actually be measured, and the X-ray data can be utilized to analyze the velocity distribution of the energetic electron tail.

The techniques were originally developed in order to analyze runaway discharges on pioneering tokamaks. Nowadays, after a temporary loss of interest in this method, its renesance has come about thanks to experiments with the RF current drive investigation. It was shown that the RF current drive is connected to the formation of a hot electron tail.

With respect to the fact that the small Czechoslovak Castor tokamak is aimed mainly at research of lower hybrid current drive (LHCD) it was decided to perform systematic observations of hard X-rays on this device.

This paper forms the basis for quantitative measurements. In section 1 a brief description of the Castor tokamak is given. Section 2 deals with chosen theoretical facts that must be taken into account before beginning the experiments. Described are the conditions for the formation of runaway electrons and their distribution function is derived. Discussed are the resulting bremsstrahlung, possibilities of loss of

runaway electrons and impact of LHCD on runaway electrons, all with respect to experimental methods.

Section 3 deals with the first qualitative measurements of hard X-ray radiation on the Castor tokamak. Performed were a series of integral measurements which mapped azimutal dependance of the radiation. These measurements are discussed in section 3. It can be shown that even such a simple experiment gives a whole series of physical information. In the conclusion of this paper we hint at the next possible program of hard X-ray measurements.

1. Castor Data

The familiar star Castor, composed of 3 tight binary stars, one can find in the constellation of Gemini. But we won't talk about it though it would be surely interesting too.

Czechoslovak Academy of Science TORus is an experimental device designated for research and investigation of high temperature plasma. This Castor can be found at the Institute of Plasma Physics in Prague. It is a small tokamak with a major radius $R = 0{,}4$ m and a minor radius $a \cong 0{,}085$ m (see fig. 1), in which hydrogen plasma with a central ion temperature $T_i(0) = 50\text{-}120$ eV and a central electron temperature $T_e(0) = 200\text{-}400$ eV is confined. The length of discharge in the experiments described in sec. 3 was about 10 ms.

At the present time, after a recent reconstruction of the energy sources, the length of discharge has been prolonged up to 40 ms [4]. Plasma with a density of $n = (0{,}2\text{-}4{,}0).10^{19}$ m^{-3} is held in a magnetic field $B_T = 1\text{-}1{,}3$ T and heated by an induced toroidal current $I_p = 10\text{-}20$ kA. Both the magnetic field and the electric current are oriented counter-clock-wise.

The liner of the tokamak is made of stainless steel and its thickness is 0.5 mm. The shell is made of 10 mm thick copper torus. The copper toroidal field coils together with their dural coverings are 50 mm thick or

more. These facts must be considered in the discussion of the results in sec. 3.

The Castor tokamak is used mainly for the investigation of interactions between the high frequency electromagnetic wave at a frequency 1,25 GHz and power up to 40 kW, with plasma. The wave is launched into the plasma by means of a special multijunction antenna system (so called waveguide-grill). The grill generates a slowing-down wave in the plasma column with the phase velocity $v_\varphi < c$, which propagates predominantly in one direction. Such a wave transmits its momentum to the plasma electrons and the high energy tail forms on the electron distribution function (see fig. 7). Therefore, the asymmetry of the electron distribution results in an additional toroidal plasma current. Plasma instabilities can transfer the tail's kinetic energy into thermal energy of the plasma (see sec. 2.3).

2. Basic Theory of Runaway Processes

In this part we use and modify basic thoughts from refs. [1], [2] and [3]. Those who are interested in a deeper study of the following theory should turn to the above mentioned papers.

In all numerical approximations for the tokamak Castor we assume:

plasma density	$n = 5 \cdot 10^{18}\ m^{-3}$
electron temperature	$T_e = 300\ eV$
effective plasma charge	$Z_{eff} = 2$ $Z_{eff} = \frac{\sum_i n_i Z_i^2}{\sum_i n_i Z_i} = \frac{\sum_i n_i Z_i}{n_e}$
loop voltage	$U_{loop} = 2{,}5\ V$
electric field intensity	$E = 1\ V m^{-1}$ $E = \frac{U_{loop}}{2\pi R}$
Coulomb logarithm	$\ln \Lambda = 15$

2.1 The Creation of Runaway Electrons

On an electron of mass m moving in a fully ionized plasma with velocity u acts an electromagnetic frictional force whose magnitude can be estimated by

$$F_p(u) = m u \nu \qquad (1)$$

where ν is the frequency of Coulombical collisions [5]

$$\nu = \frac{n e^4}{16 \pi \varepsilon_0^2 m^2 u^3} \ln \Lambda \qquad (2)$$

The dependence of the correctional Coulomb logarithm on the velocity u is negligible, therefore it can be said that the magnitude of the frictional force is inverselly proportional to the energy of the electron.

By detailed calculation of mean frictional forces for an electron moving in Maxwellian distributed field particles ($mv_{th}^2 = kT_e$) we get in the first approximation (undisturbed distribution) and for $u \gg v_{th}\sqrt{m_e/m_i}$ the same result with the exception of factor f which describes the effects of impurities [1]:

$$\langle F_p \rangle_M = f \cdot \frac{n e^4}{16 \pi \varepsilon_0^2 m u^2} \ln \Lambda \qquad (3)$$

where

$$f = \frac{Z_{eff}}{2} \quad \text{for} \quad \frac{m_e}{m_i} \ll \frac{u}{v_{th}} \ll 1 \qquad f = \frac{2 + Z_{eff}}{2} \quad \text{for} \quad \frac{u}{v_{th}} \gg 1$$

Let's assume that on the moving particle acts a force F = eE in the direction of its motion. The critical velocity u_c is defined by balancing this force against the frictional drag of Coulomb collisions:

$$\langle F_p \rangle_M = eE$$

From eq. (3) can be obtained

$$u_c = \sqrt{f \cdot \frac{ne^3}{16\pi\varepsilon_0^2 mE} \ln\Lambda} \qquad (4)$$

which gives for the Castor tokamak $u_c = 2 \cdot 10^7$ ms^{-1}.

Electrons with velocities $u > u_c$ will be gradually accelerated by the electric field to high energies. On the other hand, electrons with velocities lower than u_c will remain in the thermal population. Near $u = u_c$ the electron distribution is gradually transformed from being isotropic to highly directed towards the applied electric field.

The critical electric field E_c is defined by the condition

$$u = v_{th} = \sqrt{\frac{kT_e}{m}}$$

which results in

$$E_c = f \cdot \frac{ne^3}{16\pi\varepsilon_0^2 m v_{th}^2} \ln\Lambda \qquad (5)$$

For fields $E > E_c$, thermal electrons will run away, whereas if $E < E_c$, only the tail of the distribution function is subjected to free acceleration.

The ratio

$$\frac{u_c}{v_{th}} = \sqrt{\frac{E_c}{E}}$$

results for Castor approx. 1,7 (!). The critical energy (for $u_c \ll c$)

$$W_c = \frac{1}{2} m u_c^2 \qquad (6)$$

or in practical units

$$W_c \cong 2 \cdot 10^4 \left(\frac{n_e}{10^{19}}\right)\left(\frac{0{,}1}{E}\right)\left(\frac{\ln\Lambda}{15}\right) \quad (eV;\ m^{-3}, Vm^{-1}) \qquad (7)$$

results approx. 1 keV only.

In nonrelativistic Maxwellian distributions there always exist electrons with initial velocity $u>u_c$ sufficient to cross over into runaway regime. In a relativistic distribution, runaway electrons can be produced only if the relation

$$\frac{E}{E_c} \gtrsim \frac{kT_e}{mc^2} \qquad (8)$$

is fulfilled.

The kinetic theory of runaway production in plasma subjected to a weak applied electric field ($E<<E_c$) has been examined by numerous authors over the past 30 years. For the most part, these calculations assume an infinite, homogeneous, quasi-steady-state, non-relativistic plasma, with a distribution function close to Maxwellian, and neglect collective effects. In more recent work, relativistic effects and the influence of toroidal geometry have been examined.

The results of some key papers on this topic are given in fig. 2; λ represents the rate of diffusion of electrons into the runaway state:

$$\frac{dn}{dt} = -\lambda \qquad (9)$$

where n is the density of electrons with subcritical velocity (quasi-steady-state).

Perhaps the most consistent and rigorous treatment of the runaway production problem was presented by Kruskal and Bernstein [6] and Gurevich and Zhivlyuk [7]. They were able to obtain the runaway rate as a function of the electric field up to an unknown normalization constant K. Calibration of this undetermined constant was provided by a numerical solution of the Fokker-Planck equation by Kulsrud et al. [8]. After correcting for impurities by Cohen [9] and for relativistic effects by Connor and Hastie [10], the

resulting equation is:

$$\lambda = K(Z_{eff}) \left(\frac{E_c}{E}\right)^{\frac{3(Z_{eff}+1)}{16}} n\nu(\nu_{ei}) \exp\left[-\frac{E_c}{4E} - \frac{(Z_{eff}+1)E_c}{E}\right] \exp\left\{-\frac{kT_e}{mc^2}\left[\frac{1}{8}\left(\frac{E_c}{E}\right)^2 + \frac{2}{3}\left(\frac{E_c}{E}\right)^{\frac{3}{2}}\sqrt{1+Z_{eff}}\right]\right\} \qquad (10)$$

The last exponential term is the relativistic factor. The effects of the toroidal magnetic field (see sec. 2.3) needn't be taken into account for typical tokamak parameters [11].

Eq. (10) gives the possibility of preassuming the radial profile of runaway electrons, if one knows the density and temperature profiles, or vice versa.

The calibration constant K has an approximative value of $K = 0{,}5$ at $Z_{eff} = 2$. In the case of the Castor tokamak the resulting value of the runaway rate is of order

$$\lambda \simeq 10^{21} - 10^{22}\ m^{-3}s^{-1}$$

(the Coulomb collision frequency ν is approx. 50 000 s^{-1}), but the above mentioned assumptions for (10) are not well-fulfilled, namely the assumption for $E \ll E_c$. Consequently, the assumption for a distribution function close to Maxwellian is doubtful due to the low critical energy (7).

It is important to note, that for energies $W = \frac{1}{2}mu^2 < 70$ eV the momentum transfer cross-section (and therefore also the frictional force) is smaller for partially ionized gasses than for fully ionized gasses. Thus as long as the gas is not fully ionized, the critical velocity is lower.

Qualitatively, the consequence of this effect during the breakdown phase (together with higher U_{loop}) is the production of a relatively larger number of runaway electrons. A quantitative evaluation of this effect is practically impossible, because one should take into account the particular experimental conditions with their time and radius dependences.

2.2 The Runaway Electrons Distribution Function Bremsstrahlung of the Runaway Electrons

For experimental observation of runaway electrons using hard X-ray radiation it is crucial to know what kind of photon spectrum will the given distribution function of these electrons induce.

The electron distribution function can be estimated by a simple procedure, modified according to [2], with fairly strong, but quite realistic assumptions.

The distribution $f(p_1,t_1)$ in a fixed time t_1 will be considered with the condition, that this distribution originates in a time interval $t_0<t<t_1$ by supplying runaway electrons with momentum p_0 at a rate of $\dot{n}(t)$ particles per second. Further assuming, that these particles are moving in the considered time interval entirely without interaction with their surroundings, i.e. that they form a free-fall distribution.

This assumption is well fulfilled in the region of runaway electrons velocity which is considerably higher than the critical one, i.e. for the initial condition $p_0 >> mu_c$. Thus, it cannot be expected that the value of $\dot{n}(t)$ will coincide with the theoretical value according to (10); on the contrary, comparing these two values it may be possible to estimate the diffusion of lower-energy runaway electrons.

The magnitude of the only force acting on the electrons in the free-fall distribution is given by

$$F = \frac{dp}{dt} = eE(t) \qquad (11)$$

The number of particles at a time t_1 in a momentum interval (p_1, p_1+dp_1) is $f(p_1,t_1)dp_1$. The same amount of particles were in the region $(p,p+dp)$ at a time t, as long as

$$p_1 - p = \int_t^{t_1} eE(t')\,dt' \qquad (12)$$

holds. Thus

$$f(p_1,t_1)dp_1 = f(p,t)dp \qquad (13)$$

is valid.

Becouse the change in momentum is not a function of momentum, the magnitude of the differential of momentum is conserved in time:

$$\Delta p_1 = p_{A_1} - p_{B_1} = p_{A_0} + \int_{t}^{t_1} eE(t')dt' - p_{B_0} - \int_{t}^{t_1} eE(t')dt' = p_{A_0} - p_{B_0} = \Delta p$$

for any distance between boundaries A and B. Therefore

$$dp = dp_1 = dp_0$$

Notice, that the analogy does not hold for the differential of time in momentum space.

In any moment the number of particles in an interval (p_0, p_0+dp_0) equals

$$f(p_0, t)\, dp_0 = \dot{n}(t)\, dt \qquad (14)$$

which means that all other particles, except for these just supplied, were driven by the field into higher regions of momentum.

According to (11), (13) and (14) we can write the final system of equations for independent variables p_0, t_1, p_1:

$$f(p_1, t_1) = \frac{1}{e\,E(t)}\, \dot{n}(t) \qquad (15)$$

where t is determined by

$$p_1 = p_0 + \int_{t}^{t_1} eE(t')dt' \qquad (16)$$

According to this, the region p_1 is limited by:

$$p_0 \leq p_1 \leq p_0 + \int_{t_0}^{t_1} eE(t')\, dt'$$

As long as it is assumed that runaway losses are stationary and proportional to their rate of creation, the relation between $\dot{n}(t)$ and $E(t)$ is determined by equation (10). A more fertile and often experimentally acceptable is a more stringent assumption, that the discharge is stationary also in electric field intensity and in the runaway production rate (i.e. furthermore according to (10) and (5) it is also stationary in density and temperature). Then holds

$$\begin{aligned} &f(p_1 < p_0,\ t_1) \quad \text{undefined} \\ &f(p_0 \le p_1 \le p_0 + (t_1 - t_0)eE,\ t_1) = \text{const.} \\ &f(p_1 > p_0 + (t_1 - t_0)eE,\ t_1) = 0 \end{aligned} \tag{17}$$

The corresponding maximum energy of the distribution is

$$\mathcal{E}_m = \sqrt{[p_0 + (t_1 - t_0)eE]^2 c^2 + (m_0 c^2)^2} \tag{18}$$

The distribution function according to (17) has from an experimental point of view two basic advantages:

a) It is relatively easy to find numerically the resulting spectrum of the bremsstrahlung emission from the bremsstrahlung spectrum induced by a single electron. The latter was derived for fully ionized plasma by Kramer [12], the relativistic effects were taken into account by Koch and Mott [13], the exact cross sections by Pratt [14].

b) The bremsstrahlung spectrum is bound from the top by the maximum electron energy $\mathcal{E}_m$. Therefore, by fitting from the top the theoretical bremsstrahlung spectra of a free-fall distribution of electrons on a measured spectrum, this can be identified as a superposition of spectra of type (17). It is therefore possible to determine experimentally in several points the actual course of the distribution function of runaway electrons. Using eq. (15), (16) and the voltage course the actual rate of supplying electrons

$\dot{n}(t)$ can be then estimated.

The energy spectrum of bremsstrahlung in the case of the simplyfied free-fall distribution function taken from [2] is given in figure 3. In fig. 3(a), the beam of electrons is observed by a detector at an angle of 60° to the beam direction. Spectra for 90° have a very similar shape but somewhat smaller intensity. In fig. 3(b) the beam is observed at 3° to the beam direction. Two features of these graphs merit attention:

a) The spectra shown in fig. 3(a) fall off approximately in an exponential fashion. This fact can easily lead to misinterpretation of the experiments: An exponential photon spectrum does not necessarily imply an exponential velocity-distribution function.

b) A comparison of fig. 3(b) with (a) shows that the X-ray emission peaks in the forward direction, as can be expected, i.e. the tangential emission is produced predominantly by the most energetic particles. For the 60° or 90° view, the relative contribution of the very energetic particles is reduced and, therefore, the perpendicular view seems better suited for measuring the whole course of the distribution function of the electrons including the low energy part.

Experiments which were carried out using this method on the ST tokamak are described in great detail in [2]. One representative example is given in fig. 4:

The figure shows a time sequence of three consecutive hard X-ray spectra for two discharges labelled (a) and (b). A free-fall curve has been fitted on the first spectrum measured at 14 ms. Since the loop voltage is known, one can calculate how the spectrum should develop in time using eqs. (15) and (16). The corresponding free-fall spectra for times t = 27 ms and 40 ms are also plotted in the figure. The experimental spectra at 27 ms and 40 ms do not seem to expand toward the higher energies, rather they seem to saturate. It has been proposed that this behaviour is caused by radial transport of runaway electrons across the magnetic field (see Sec. 2.3). A confinement time τ of

the runaway electrons can be estimated by calculating the time that it takes for an electron to free-fall to an energy $\mathcal{E}_c$, the value that provides a good fit to the saturated spectrum. A variety of data for the runaway confinement time from ST has been plotted in fig. 4(c).

The bremsstrahlung spectra for relativistic Maxwellian distributions of runaway electrons are plotted in [2] too (in addition there is a factor of space angle which occupies the tail of electrons). The numerical calculations of bremsstrahlung spectra can be performed for any distribution of runaway electrons, but in practical cases quasiexponential dependences of bremsstrahlung spectra are always obtained. The real shape of the runaway electrons distribution function can be determined only by measurements of hard X-ray radiation as a function of angle with respect to the magnetic field. Such measurements would be complicated by the absorption of the radiation in plasma and by the construction of the tokamak vessel.

2.3 Confinement of Runaway Electrons

A brief discussion of the confinement of runaway electrons follows. A more detailed, quantitative analysis of this problem is dealt with in [1] and especially in [3].

From the single-particle view we needn't include the interaction of high energy electrons with plasma, but it is not possible to omit drifts of the particle in toroidal geometry. Especially due to grad-B drift and centrifugal drift the high energy electrons are declined outwards from the plasma column. In axisymmetrical fields the limiter defines the actual shape of the high energy electron beam. A numerically calculated drift surface of runaway electrons is shown in fig. 5 for the current profile $j=j_0(1-(r/r_L)^3)$ and total current as indicated. The kinetic energy starts at 2 MeV (outermost orbits) and goes up by 2 MeV increments.

The loss of runaway electrons is then given by the interaction with the liner or limiter, with respect to

the growing drift due to the growing energy.

From the many-particle models point of view, for example fluid model, it is not possible to omit the free energy, which is represented by the kinetic energy of high energy electrons against the Maxwellian plasma. Therefore an interaction between the high energy electrons and plasma via beam instability must be expected. This case of instability is called fan-like instability or anomalous Doppler instability. This instability may include current steps, voltage spikes, inward shifts in the plasma position, density fluctuations, bursts of hard X-rays, sudden increases in the emission of microwaves, and anomalous resistivity.

A typical electron velocity distribution before the fan-like instability (solid curve) and after it (dashed curve) is in fig. 8; (a) is the distribution with respect to $v_{\parallel}$, (b) is the distribution in the $(v_{\parallel}, v_{\perp})$ plane [1]. The instability occurs, when the degree of distortion by runaway electrons exceeds a certain critical level. Elecrostatic waves are excited at Doppler-shifted harmonics of the gyrofrequency in this case; the two most important are the Cerenkov resonance and the anomalous Doppler resonance [1]. The former scatters electrons predominantly in energy, the latter in pitch-angle.

The instability excites a very broad spectrum of waves, which act to isotropize the beam part of the distribution function. In consequence, the instability is cut off. After saturating, the runaway tail builds up again to the point, where the instability cycle will be repeated.

As a result of anomalous Doppler resonance, a part of runaway electrons is pitch-angle scattered. If the pitch-angle

$$\chi = \operatorname{arctg} \frac{v_{\perp}}{v_{\parallel}} \qquad (19)$$

is large enough, the electrons are trapped in the grad-B mirrors in "banana" orbits (see fig. 6a,b). The electrons slowly drift upwards (or downwards) along grad-B drift surfaces, until they collide with the liner

or the limiter or with plasma ions. From a more realistic point of view, the electrons are trapped in the local mirrors between the toroidal field coils as well. Hence, the trajectory of a trapped electron is not axisymmetrical. The drift velocity is not compensated during the excursion of the electron then; the electron thus drifts out of the plasma into the wall (see fig. 6c), where strong bursts of hard X-rays originates, connected with fan-like instability.

These colisionless interaction phenomena associated with runaways are of interest in order to eliminate energy losses and to avoid liner damage, which results from direct electron drift to the walls. Finally, it is interesting to note that the instabilities excited by runaway tail were proposed for supplementary heating at high temperatures, where Ohmic heating is already ineffective.

2.4. Plasma Bremsstrahlung during LHCD

X-ray techniques have shown that a fast electron tail forms soon after the RF is switched on [2], see figs. 7, 9. After about 30 ms its evolution is completed and a stationary electron distribution is estabilished provided that the discharge condition are kept constant.

During the RF pulse, the energetic electrons have to carry practically the total plasma current, because the loop voltage (and consequently the inductive current drive) vanishes. The radial X-ray profile should also contain information on the location of the current in the plasma. An exact evaluation of the current from X-ray profiles requires a large data base: the energy distribution in the tail has to be known as a function of radius. For a preliminary estimate it can be assumed, that the X-ray intensity is proportional to the number of energetic electrons. If, in addition, their average velocity does not vary significantly with radius, then it is not unreasonable to assume that the X-ray profiles represent current density profiles. Equating the X-ray profiles with the current profiles,

q-profiles can be calculated.

According to [2], when the toroidal magnetic field is decreased and/or when the plasma current is increased, the X-ray profiles consecutively broaden. It was also observed, that the X-ray profile, once it was established, remained unchanged for the rest of the RF pulse. The creation of energetic electrons seems to produce a plasma of high conductivity in which the current profile seems to be frozen in.

Experiments, in which the RF power was varied have shown, that there exists saturation of the hard X-rays intensity with power. The RF fields seem to create a diffusion in velocity space that favours the creation of modestly energetic electrons and eliminates very high energy electrons (see fig. 10). The first indication of this effect is the reduction of hard X-ray radiation with the onset of the RF power.

Another factor that influences the slope of the X-ray tails is the phasing of the waveguides of the grill. The phasing, which gives a more efficient LHCD, gives generally a flatter hard X-ray spectrum. It is so, because the current drive with more effective phasing gives a higher phase velocity of the electromagnetic wave in plasma, with which than interact runaway electrons.

Quasilinear theory predicts that f(p)=const in a strong RF field. On the other hand, it was shown in fig. 9 that the X-ray spectra can also be described by a free-fall distribution f(p)=const . What might be seen with the X-ray spectra is just the distribution function f(p)=const with boundaries ξ_m according to Brambilla theory [15] for wave propagation parallel to the magnetic field.

The validity of the assumption f(p)=const might be confirmed by measuring the hard X-rays at different angles with respect to B.

The transfer of RF power at the electron cyclotron frequency to runaway electrons has been studied theoretically in [16].

3. Experimental Results

A layout of the hard X-ray detector for the following experiments is shown in fig. 11. The detector used in this experiment is a small photomultiplier with ø40x30 mm NaI(Tl) scintilator which is shielded by 50 mm of lead. In the front wall of the shielding is an opening of diameter 7 mm which allows us to observe a circular area of ø200 mm on the torus. During these experiments it was not possible to observe the plasma column directly. The measured radiation was the radiation which penetrated the torus shell or which was induced in it.

As a consequence of the high intensities of radiation flux its discrete character vanishes and the detector output gives a sum of many pulses. The photomultiplier was connected directly to a data acquisition system, because the detector pulse decay itself (about 4 μs) is a suitable integration constant. The measurements presented here are therefore simple in principle and bring primarily qualitative information about discharge radiation in the hard X-ray region only.

The azimutal dependence of hard X-ray radiation was measured in 8 basic positions with similar constructional consistency of the torus (except pos. 4, with vacuum system's pipes in the view), during four different regimes of discharge and at two different energy ranges. However, the energetic ranges do not have well defined limits. These are approximately defined as:

1) measurements in the entire range of the detector, approx. 30 keV - 1.5 MeV.

2) measurements taken with a 4 mm lead absorber (which absorbs the lower energetic regions of the hard X-rays). This layer of Pb lowers the intensity of the 270 keV X-rays ten fold (this value is derived from a table of absorption coefficients from [17]). At 400 keV more than a third of the radiation penetrates this

absorber.

It is important to keep in mind that the measurements of radiation were performed with the detector directed towards the shell of the tokamak, where a large amount of softer rays is absorbed. Therefore it is important to take into account the fact that the low energy component of hard X-rays is produced in a noticeably higher rate than the observed one.

Absorption in the 0.5 mm Fe liner can be ignored. The energies, which decrease after traversal the 10 mm copper shell 10 or 100 fold, according to [17], are 130 keV or 100 keV respectively. The dural coils, which are in the detector viewing angle as well, reduce the energies of 90 keV or 50 keV (similarly as above). Absorption in 1.5 m of air for energies higher than 30 keV can be neglected.

(i) The discharge regime without feedback stabilization of the plasma column

The first measured regime is characterized by the loop voltage and plasma density evolutions according to fig. 12 (reprinted here are only typical cases of the given discharge regime). In fig. 13 is shown the evolution of hard X-ray radiation monitored during the first and last discharge of the series by an unshielded detector of the same type, situated permanently above the tokamak. In the figure can be seen an increase of radiation. The cause of this increase can be interpreted as an increase in impurities. It is important to take into account this effect during the evaluation of results, which are in fig. 14. The measurements were taken from positions 1 to 8.

(ii),(iii) The discharge regime with feedback stabilization of the plasma column

(iii) The discharge regime with application of the RF wave

In the measurements which followed two discharge regimes were compared, both with feedback stabilization of the plasma column. Besides the discharges with standard Ohmical heating, the regime with application of

lower hybrid wave (from the fourth to the sixth miliseconds) was examined. These two regimes were repeatedly alternated so that the results could be meaningfully compared. Regimes are characterized by loop voltage and plasma density according to fig. 15 (dashed line - without current drive, full line - with current drive). The comparative measurements of hard X-ray radiation are in fig. 16. The results of azimutal measurements of the hard X-ray radiation are shown in fig. 17 (without current drive) and in fig. 18 (with current drive). Position 7 was not accessible because of the installed diagnostic system for soft X-rays.

In fig. 17 in positions 1, 2, 6 and 8 is very noticeable sharp increase in the intensity of the soft component of radiation during the time interval of 5-6th ms. In the same instant the same increase arises in positions 6, 7 and 8 during the regime without feedback stabilization (fig. 14). During LHCD is the increase of intensity of the soft component noticable in position 6 already during the 4-5th ms (fig. 18). It is very probable that this is a consequence of the fan-like instability, see sec. 2.3. The electrons with high perpendicular energy are produced in this case. They hit the liner wall and this causes the observed bremsstrahlung. It is interesting to note that according to our azimutal measurements this phenomenon has a local character. With this method it is probably possible to indicate the magnetic field and/or liner asymmetries. Further, the comparison of pos. 6 in the figures could mean that the fan-like instability may be induced by the lower-hybrid wave propagation. For more detailed measurements of fan-like instability it will be also important to measure loop voltage spikes and emission of microwaves accurately.

The assumption in sec. 2.4. that LHCD suppresses the intensity of hard X-rays was not confirmed. It would be advantagious to repeat these measurements because the assumption may be true if the LHCD is switched on after the fan-like instability unfolds.

The azimutal dependences of hard X-rays in fig. 14 are for better interpretation redrawn in fig. 19. Here the radial coordinate is the mean intensity of hard

X-ray radiation, at three different instances of the discharge. So that measurements of individual regimes can be compared, the chosen times were related towards the end of the discharge. The last instance depicts the situation shortly before the rapid increase of radiation, induced by the decay of the plasma column. The dashed lines describe the sections where it was not possible to obtain reliable results. The evolution of hard X-ray radiation with and without LHCD are practically the same (with respect to intensities), and to them corresponds fig. 20.

Above all the preassumed strong limiter radiation can be seen from figs. 19, 20. It is also very notable that just before the plasma decay the radiation grows in the backward direction to the limiter (with regard to electron motion). It may be that the runaway electrons hit a greater part of the limiter in consequence with worse confinement.

When comparing figs. 19 and 20 one can see that the intensive limiter radiation starts later with feedback stabilization that without. This fact probably indicates, that the high-energy electrons reach the limiter later, because the plasma column is better centralized in the torus.

The increase of intensity on the south-east side of the tokamak is of uncertain origin, especially the presence of the hard component during the regime without feedback stabilization. The limiter in this place is reliably shielded by the iron yoke of the transformer. Several measurements confirmed the repeatibility of this signal. Probably the trapped high energy electrons due to some magnetic field or liner asymmetries (may be very small) intersect the liner mainly here (see sec. 2.3).

Several results, e.g. at positions 2 and 3 in figs. 17 and 18 once again stress the fact that these measurements are only of a qualitative character. The signal of the harder component in these positions in the instant of decay is significantly higher than total signal, which is obviously not possible. When measuring the total signal the photomultiplier is probably saturated.

Also the theoretical considerations (see sec. 2.2) imply the unavoidability of hard X-ray spectrometry in determining quantitative results of runaway electrons.

Conclusions

The preliminary measurements given above shall act as the motivation for future hard X-ray studies on the Castor tokamak. Even such a simple method has been able to improve our knowledge of runaway phenomenon on the Castor tokamak, though any analogical experimental report was not at our disposal. Anyway, it is quite difficuilt to compare and understand the results.

It was shown in sec. 2 that spectroscopic measurements of hard X-rays promise to obtain new quantitative results. For this purpose a hard X-ray specrometer was constructed at tokamak Castor, see fig. 21. The detection unit consists of a cylindrical ϕ100x50 mm NaI(Tl) scintillator with photomultiplier shielded with 100 mm (head on 150 mm) lead. This detector was calibrated beforehand and shows good linear properties in the region of approx. 50 keV to 2 MeV with 10% resolution and 2 μs pulse length. The detector observes the plasma through a teflon window perpendicular to the magnetic field with the possibility to scan the entire cross-section of the plasma column. The window is fully shielded from the limiter and azimutal measurements confirm that the plasma radiation is representative in this region.

The possibility of measuring the plasma radiation directly may be proved in the near future. Even in the case of negative results (the discharge length and plasma density are still rather small) some interesting spectral information may be expected for instance concerning radiation from the liner or from some material located at the edge of the plasma (see e.g. [18]).

Acknowledgements

I would like to thank all emploees at the Castor tokamak for their systematic help and advice. I am especially grateful to Petr Magula, who helped me perform all of above presented measurements and gave me concrete advice, and to dr. Jan Stöckel for his numerous physical remarks. My personal thanks also belongs to Jan Dvořák, who did the technical illustrations, and to my school-mate MIW, who helped me with the English translation of the presented paper.

References

[1] Knoepfel, H., Spong, D. A., Nucl. Fusion 19 (1979) 785: Runaway Electrons in Toroidal Discharges

[2] von Goeler, S. et al., Princeton University report No. PPPL-2010 (1983): X-ray Analysis of NonMaxwellian Distributions (Current Drive)

[3] Parail, V.V., Pogutse, O.P.: Uskorennye elektrony v tokamake; in: Voprosy teorii plazmy, vypusk 11, ed. by Leontovich, M.A. and Kadomcev, B.B. (Energoizdat, Moskva 1982), 5 (in Russian)

English version: Parail, V.V., Pogutse, O.P.: Runaway Electron in a Tokamak; in: Rewiews of Plasma Physics, vol. II, ed. by Leontovich, M.A. (Plenum Press, New York 1986) 1

[4] Valovic, M., Cs.Institute of Plasma Physics report No. IPPCZ 295 (1989): An Ohmic Heating Circuit for the Castor Tokamak

[5] Chen F.F. : Introduction to Plasma Physics (Plenum Press, New York 1974)

[6] Kruskal, M., Bernstein, I.B., Phys. Fluids 7 (1964) 407: Runaway Electrons in an Ideal Lorentz Plasma

[7] Gurevich, A.V., Zhivlyuk, Yu.N., Sov. Phys.-JETP 22 (1966) 153: Runaway Electrons in a Nonequilibrium Plasma

[8] Kulsrud, R.M., Sun, Y.C., Winsor, N.K., Fallon, H.A., Phys. Rev. Lett. 31 (1973) 690: Runaway Electrons in a Plasma

[9] Cohen, R.H., Phys. Fluids 19 (1976) 239: Runaway Electrons in an Impure Plasma

[10] Connor, J.W., Hastie, R.J., Nucl. Fusion 15 (1975) 415: Relativistic Limitations on Runaway Electrons

[11] Gurevich, A.V., Dimant, Y.S., Nucl. Fusion 18 (1978) 629: Kinetic Theory of Runaway Production in Toroidal Magnetic Devices

[12] Brussard, P., van de Hulst, M., Rev. Mod. Phys. 34, (1962) 507

[13] Koch, M.W., Motz, J.W., Rev. Mod. Phys. 31, (1959) 920

[14] Pratt, R.H., in Inner Shell and X-ray Physics of Atoms and Solids, ed. by Fabian D., Kleinpoppen, H., Watson, C. (Plenum Press, New York, 1981)

[15] Brambilla, M., Nucl. Fusion 16, (1976) 47

[16] Klima, R., Parail, V.V., J. Plasma Phys. 17 (1977) 543: Quasi-Linear Relaxation of Runaway Electrons in a HF Heated Tokamak Plasma

[17] Robouch, B.V., Cicerchia, A., CNEN report No. 80.55 (1980): X-ray Mass Absorption Coefficients...

[18] Fussman, G., Sesnic, S., IPP Munchen report No. III/37 (1977): Investigations of Runaways in the Pulsator Tokamak

[19] Arcimovic, L. A. : Ustanovki tokamak; in: Atomnaja fizika i fizika plazmy (Nauka, Moskva 1979), 98 (in Russian)

[20] Stöckel, J., Žáček, F., Czech. J. Phys. B 37 (1987): Interpretation of Toroidal Current and Loop Voltage Temporal Evolution during RF-Current Drive Experiment on the T-7 Tokamak

[21] Stöckel, J. et al., IAEA-CN-50/A-VI-3-2 : Edge Turbulence during the Combined Lower Hybrid/Ohmic Heating Regimes on the Castor Tokamak

Figure Captions

Fig. 1 : Horizontal cross-section of the Castor tokamak. (1) fixed, (2) vertically movable molybden limiter.

Fig. 2 : Electron runaway rate vs. the electric field in terms of the critical electric field. Various earlier theoretical predictions by Dreicer, Gurevich, Lebedev, and Kruskal and Bernstein predict larger rates than the experimental observations (open circles). Kulsrud and Sun succeeded in obtaining agreement in the magnitude by including the effect of impurities and also the effects of finite electron confinement. However, the confinement time seems somewhat shorter than the one shown in fig. 4. [2]

Fig. 3 : Bremsstrahlung from a beam of electrons with a free-fall distribution function (f(p)=const). Emission is given for an angle of 60° (a) and at an angle of 3° (b). [2]

Fig. 4 : A time sequence of three X-ray spectra is shown in subfigure (a) and (b) for two ST discharges. A free-fall spectrum is fitted to the spectrum measured at 14 ms, and the expected free-fall spectra for t=27 ms and 40 ms are plotted. The graph (c) shows runaway-electron confinement time τ, deduced from final stationary X-ray spectrum. [2]

Fig. 5 : Numerically calculated drift orbit trajectories that just intersect the outer limiter for the current drive $j=j_0(1-(r/r_L)^3)$ and total current as indicated; the kinetic energy starts at 2 MeV (outermost orbits) and goes up in 2 MeV increments. [1]

Fig. 6 : Trajectories of the trapped electrons: (a) projection in the poloidal plane of "banana" orbits in the axisymmetrical field; (b) the trajectory in the toroidal view; (c) the loss of the electrons trapped in the non-axisymmetrical field. The asymmetry may be caused e.g. by the finite distance between the toroidal field coils. [19]

Fig. 7 : Electron distribution function in the toroidal direction; dashed line - RF off, full line - RF on. The shift of the Gaussian occurs due to a current density $\underline{j}$ induced in the plasma. The maximum velocity of the RF driven electrons equals to the phase velocity of the RF wave. The runaway phenomena during the OH (ohmical heating) is neglected here (see fig. 8).

Fig. 8 : Typical electron velocity distribution before the fan-like instability (solid curve) and after the instability (dashed curve): (a) distribution with respect to $v_{\parallel}$; (b) distribution in the $(v_{\parallel}, v_{\perp})$ plane. [1]

Fig. 9 : X-ray spectrum with and without RF current drive at a plasma density of $6 \times 10^{18}\ m^{-3}$. The solid curves represent calculated X-ray spectra for a beam of electrons having either a Maxwellian distribution with a tail temperature of 150 keV or a free-fall distribution with maximum energy 600 keV. [2]

Fig. 10 : Hard X-ray spectra for an RF power level of 11 kW and 200 kW. [2]

Fig. 11 : The experimental layout for azimutal measurements of hard X-ray radiation at the Castor tokamak.

Fig. 12 : Loop voltage and plasma density time evolutions without feedback stabilization of the plasma column.

Fig. 13 : Comparative measurements of hard X-rays, the first measured regime: (a) The first measured discharge, which corresponds to position 1; (b) the last measured discharge, which corresponds to position 8. These measurements are carried out with an unshielded NaI(Tl) detector, situated above the south-west part of the Castor tokamak.

Fig. 14 : The resulting time evolutions of hard X-rays at different asimutes, without feedback stabilization.

Fig. 15 : Loop voltage and plasma density time

evolutions with feedback stabilization. Dashed line - LHCD off, full line - LHCD on. The drop of the loop voltage during the RF-pulse indicates that a part of the toroidal current is driven non-inductively [20]. The increase of the line-average density at the same time interval is interpreted as an improvement of the particle confinement time during the combined inductive/lower hybrid current drive [21].

Fig. 16 : Comparative measurements of hard X-rays with feedback stabilization. Dashed line - LHCD off, full line - LHCD on (see commentary on fig. 13).

Fig. 17 : The resulting time evolutions of hard X-rays at different azimutes. Feedback stabilization, LHCD off.

Fig. 18 : The resulting time evolutions of hard X-rays at different azimutes. Feedback stabilization, LHCD on from 4th to 6th ms.

Fig. 19 : This figure is derived from fig. 14 and gives a rough asimutal dependence of hard X-rays at three instances: 6 ms (initial phase), 3 ms (intermediate phase) and 1.5 ms (final phase) before the disruption of the plasma column.

Fig. 20 : This figure is derived from fig. 17, see commentary on fig. 19.

Fig. 21 : The physical layout of the hard X-ray spectrometer. (1) tokamak torus; (2) cross-section of the plasma column; (3) southern window; (4) 12 mm thick teflon (CF_2 polymer); (5), (7) movable lead apertures ϕ10 mm; (6) 100 mm lead shielding wall (8) 100 mm (head on 150 mm) lead shielding box; (9) ϕ100x50 mm NaI(Tl) detector; 100 mm of lead ensure suppressing of the hard X-rays of at least two orders (at 3 MeV, minimum of lead absorption coefficient), and e.g. approx. 2000 folds at 1 MeV.

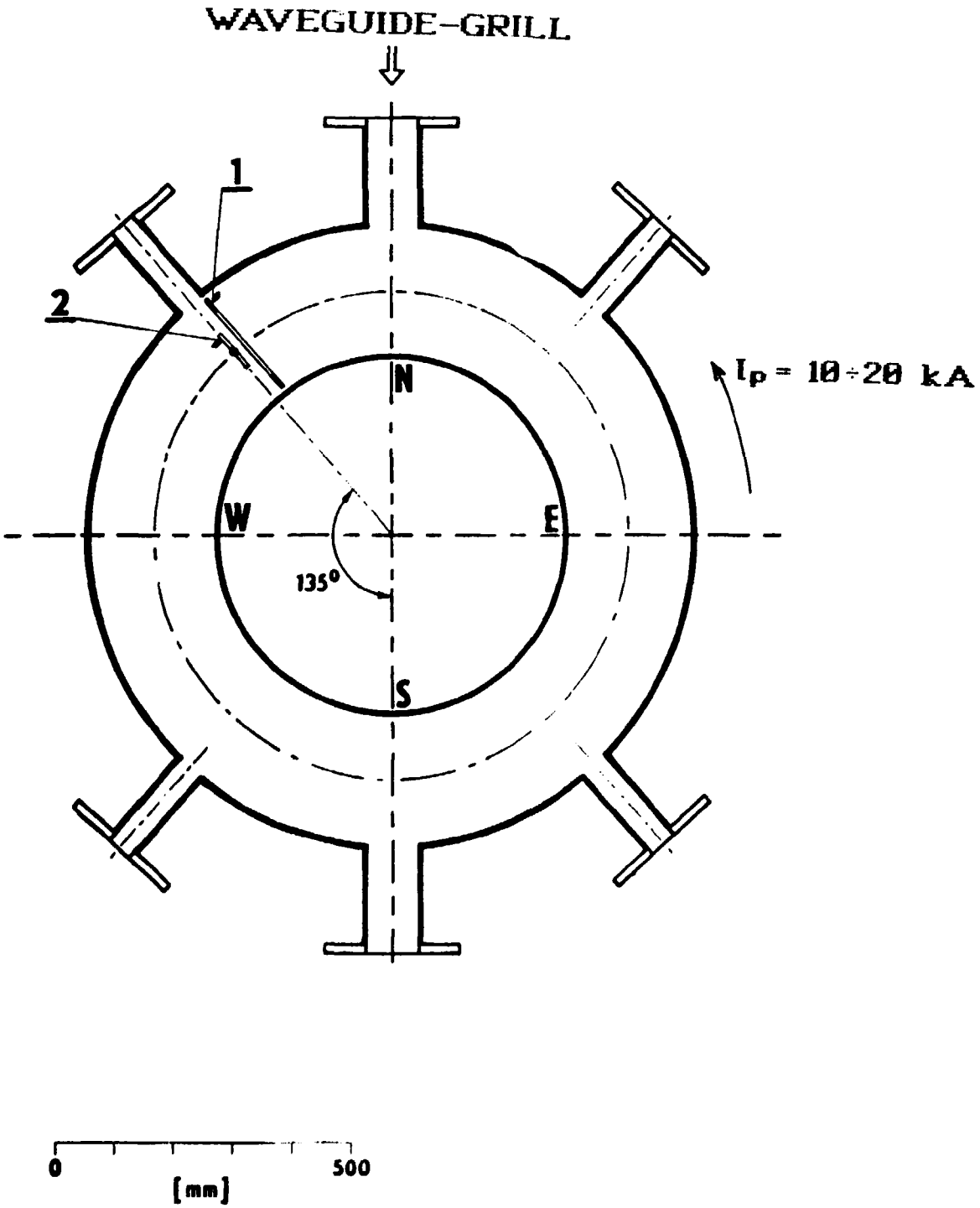

Fig. 1

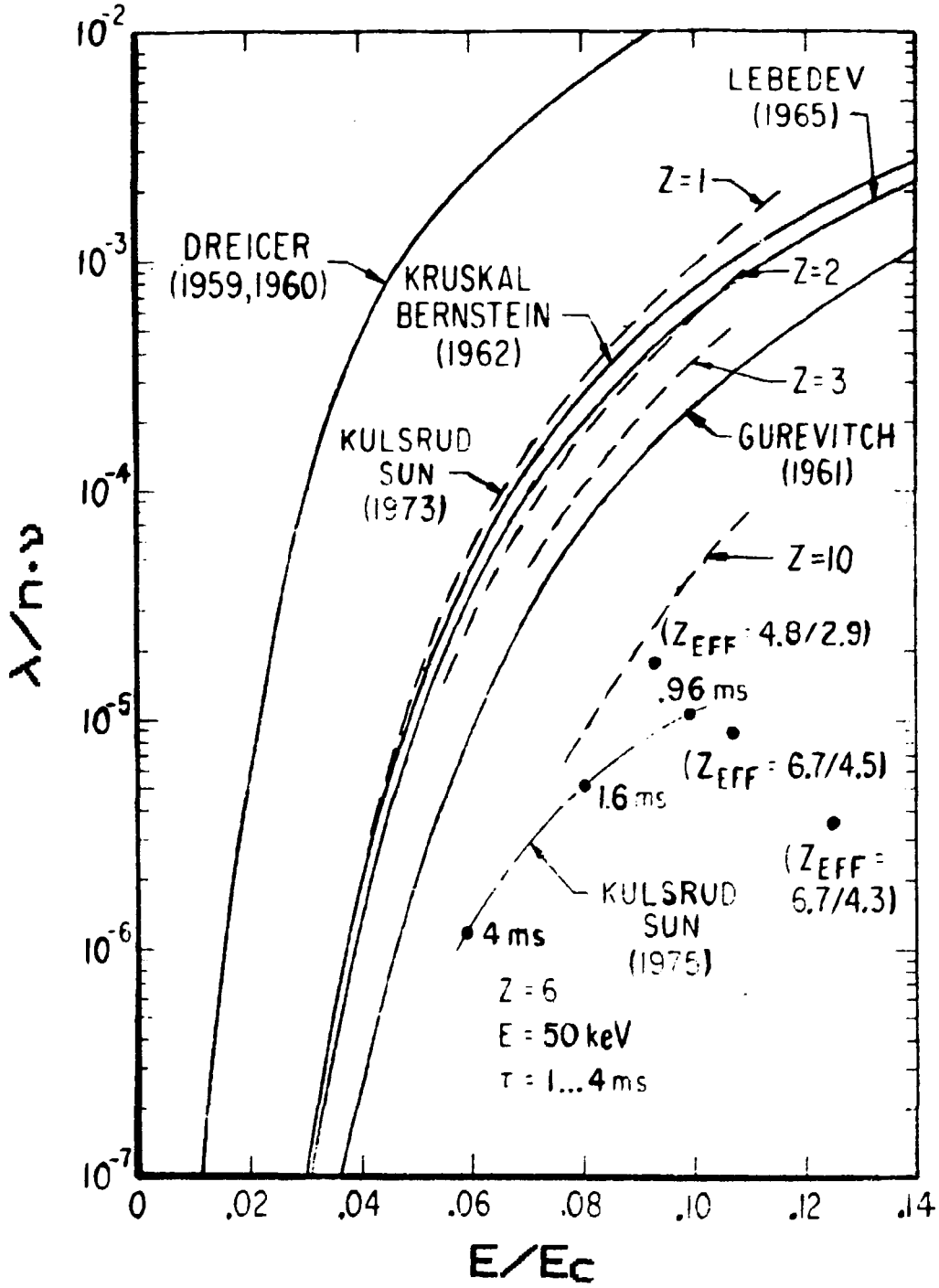
LEBEDEV
(1965)
Z=1
DREICER
(1959,1960)
KRUSKAL
BERNSTEIN
(1962)
Z=2
Z=3
KULSRUD
SUN
(1973)
GUREVITCH
(1961)
Z=10
(Z_EFF = 4.8/2.9)
.96 ms
(Z_EFF = 6.7/4.5)
1.6 ms
(Z_EFF = 6.7/4.3)
KULSRUD
SUN
(1975)
4 ms
Z = 6
E = 50 keV
τ = 1...4 ms
λ/n.a
E/Ec
10^-2
10^-3
10^-4
10^-5
10^-6
10^-7
0
.02
.04
.06
.08
.10
.12
.14

Fig. 2

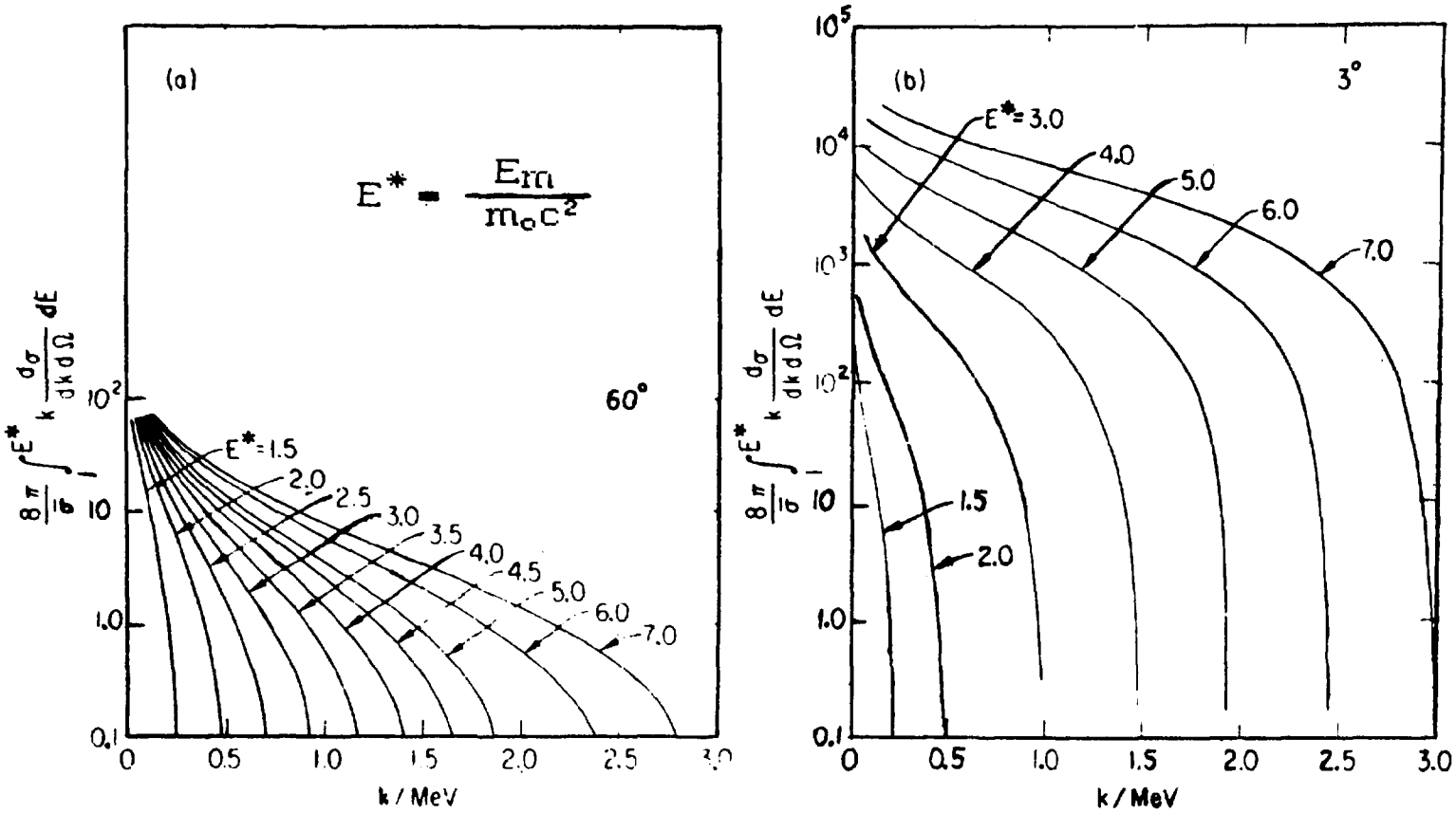
(a)
$E^* = \frac{Em}{m_0c^2}$
60°
E^*=1.5
2.0
2.5
3.0
3.5
4.0
4.5
5.0
6.0
7.0
$\frac{8\pi}{\bar{\sigma}} \int_1^{E^*} k \frac{d\sigma}{dk\,d\Omega} dE$
k / MeV
(b)
3°
E^*= 3.0
4.0
5.0
6.0
7.0
1.5
2.0

Fig. 3

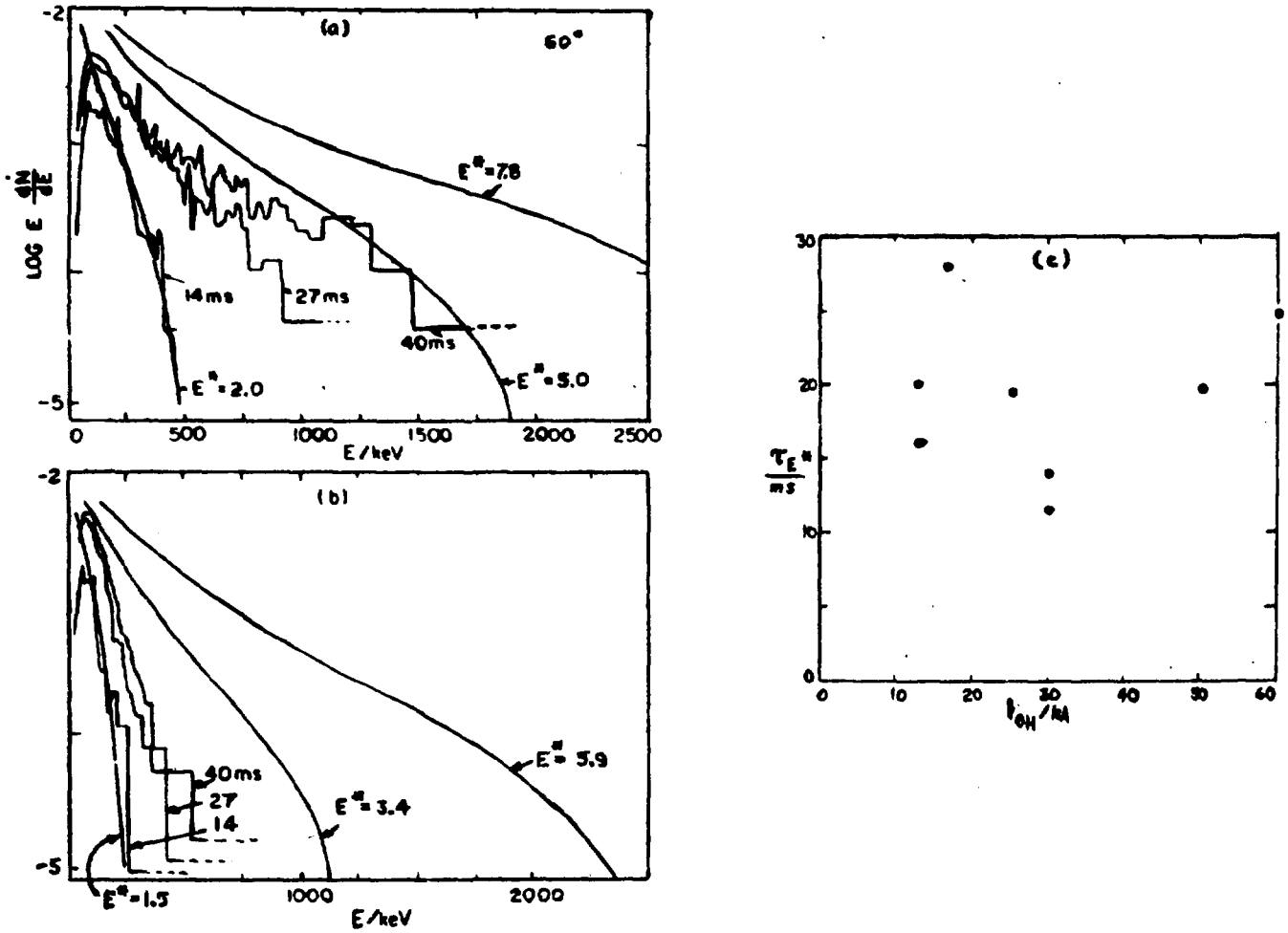
(a)
60°
E*=7.8
14ms
27ms
40ms
E*=2.0
E*=5.0
LOG E dN/dE
E/keV
(b)
40ms
27
14
E*=5.9
E*=3.4
E*=1.5
E/keV
(c)
τE*/ms
IOH/kA

Fig. 4

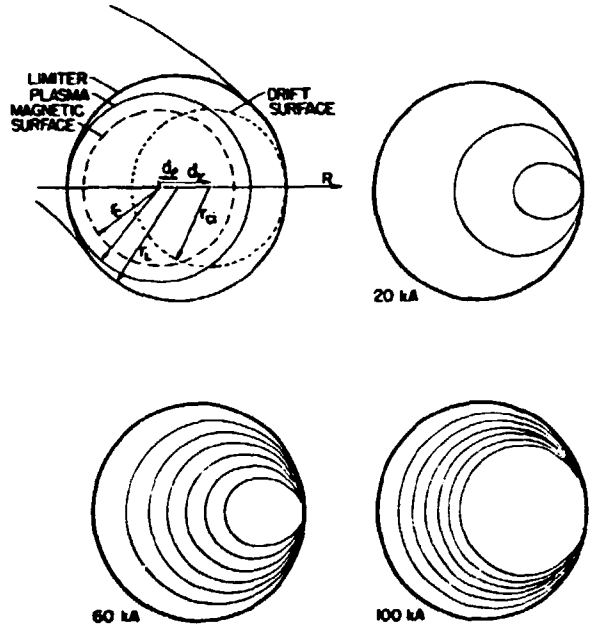
LIMITER
PLASMA
MAGNETIC
SURFACE
DRIFT
SURFACE
R
20 kA
60 kA
100 kA

Fig. 5

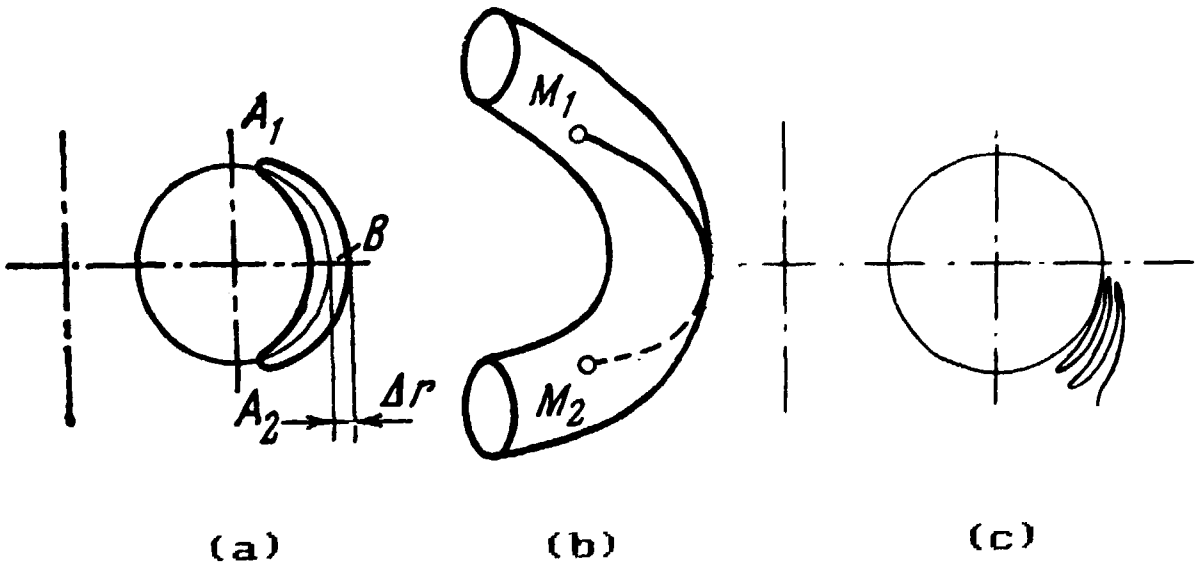
A1
B
A2
Δr
M1
M2
(a)
(b)
(c)

Fig. 6

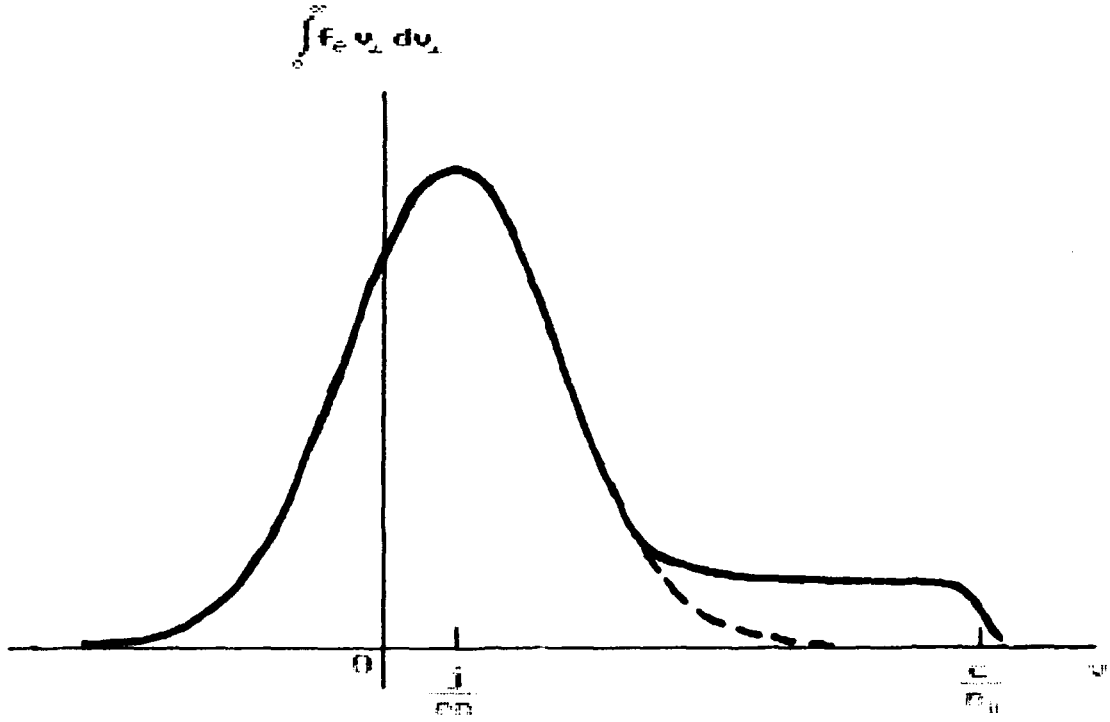

Fig. 7

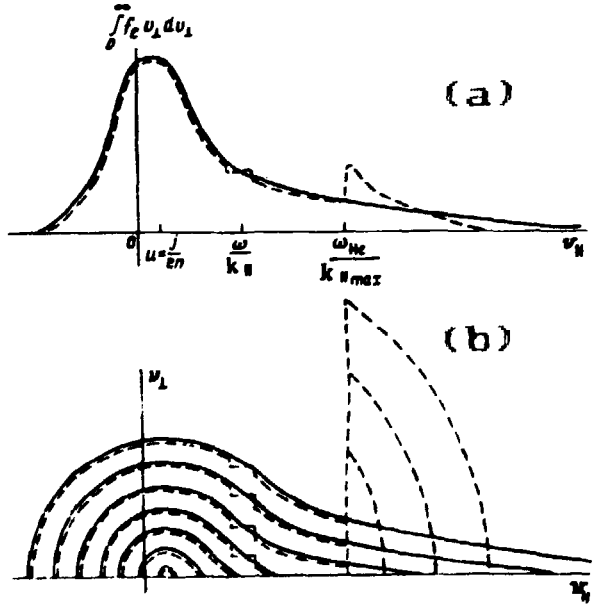

Fig. 8

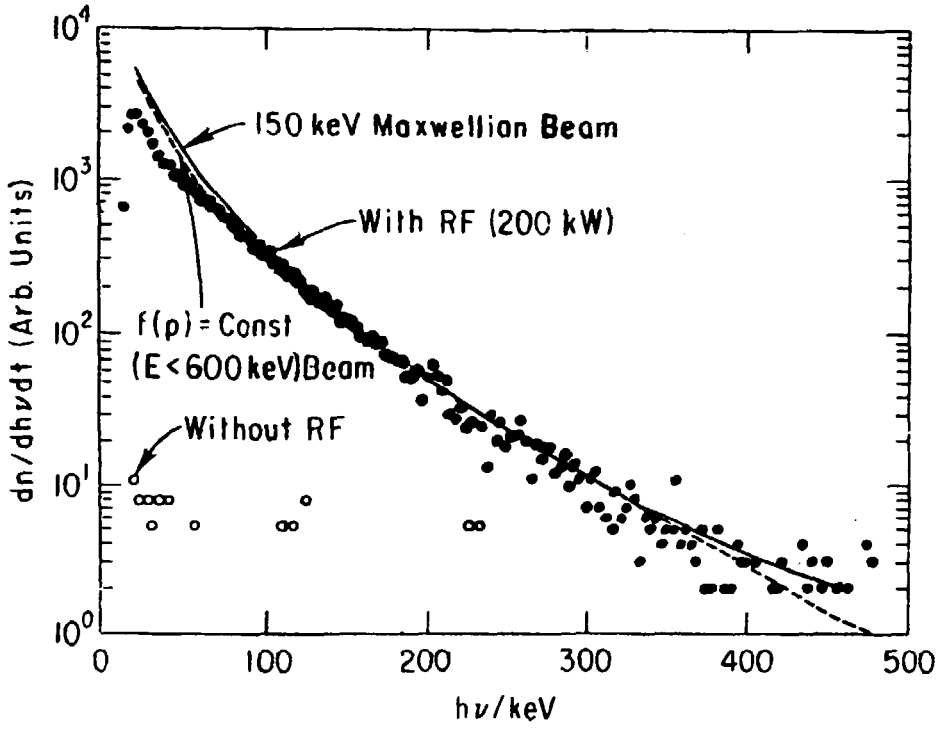
150 keV Maxwellian Beam
With RF (200 kW)
f(p) = Const
(E<600 keV)Beam
Without RF
dn/dhνdt (Arb. Units)
hν/keV

Fig. 9

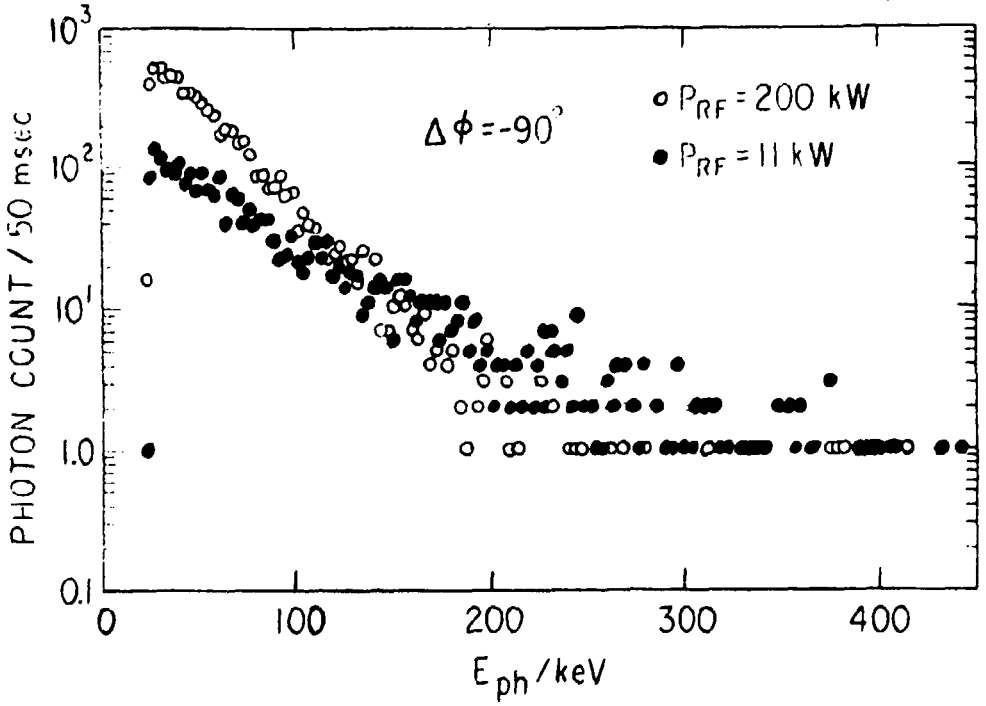
Δφ=-90°
o P_RF = 200 kW
● P_RF = 11 kW
PHOTON COUNT / 50 msec
E_ph / keV

Fig. 10

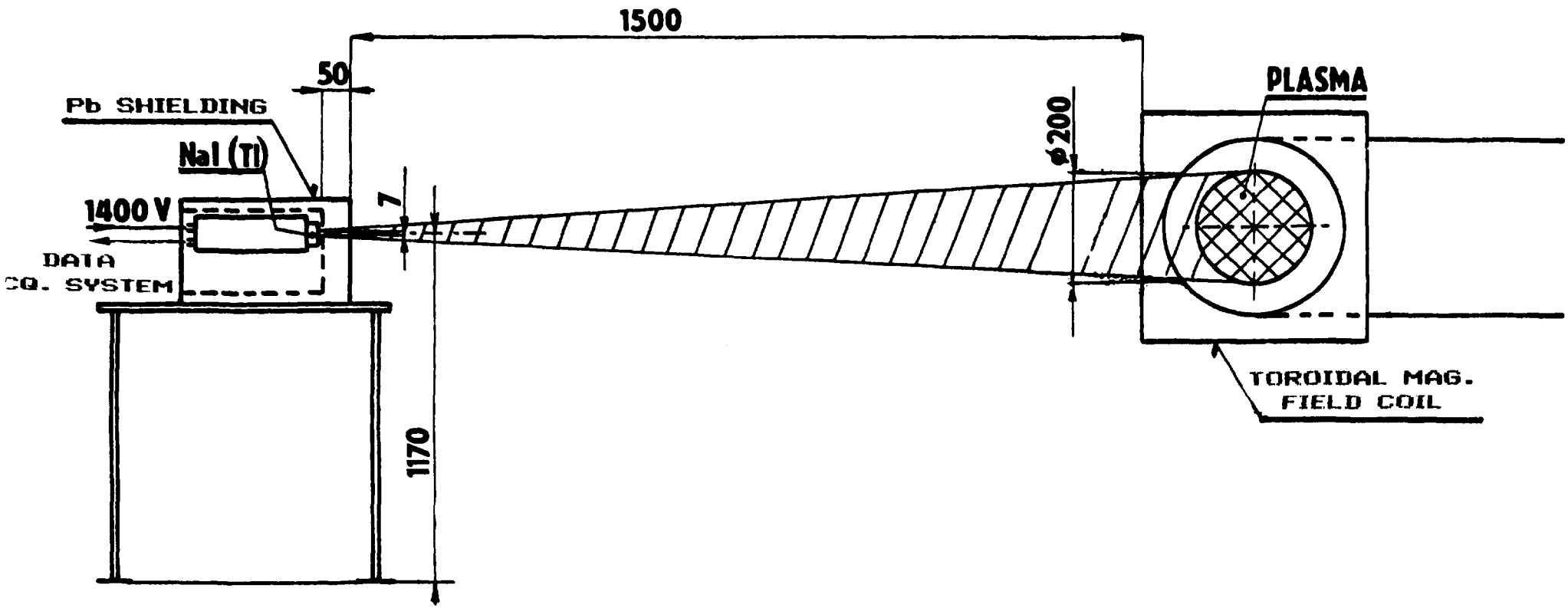
1500
50
PLASMA
Pb SHIELDING
NaI (Tl)
ϕ200
1400 V
7
DATA
CQ. SYSTEM
1170
TOROIDAL MAG.
FIELD COIL

Fig. 11

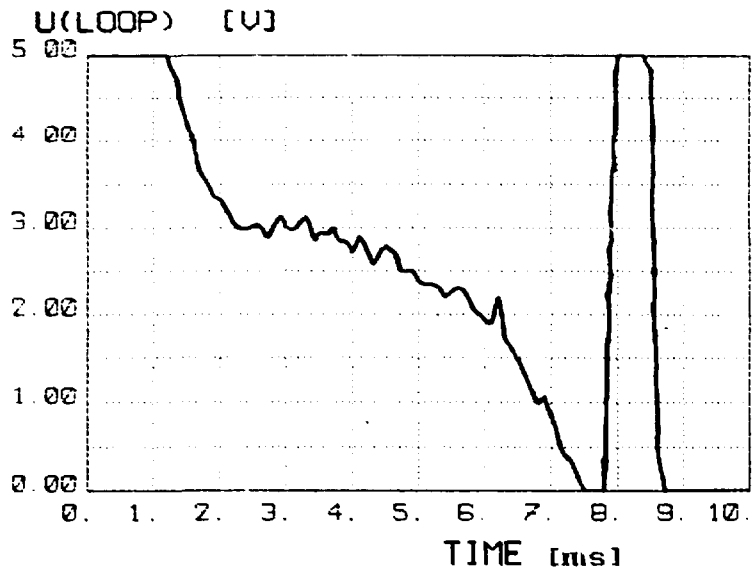
U(LOOP) [V]
5.00
4.00
3.00
2.00
1.00
0.00
0. 1. 2. 3. 4. 5. 6. 7. 8. 9. 10.
TIME [ms]

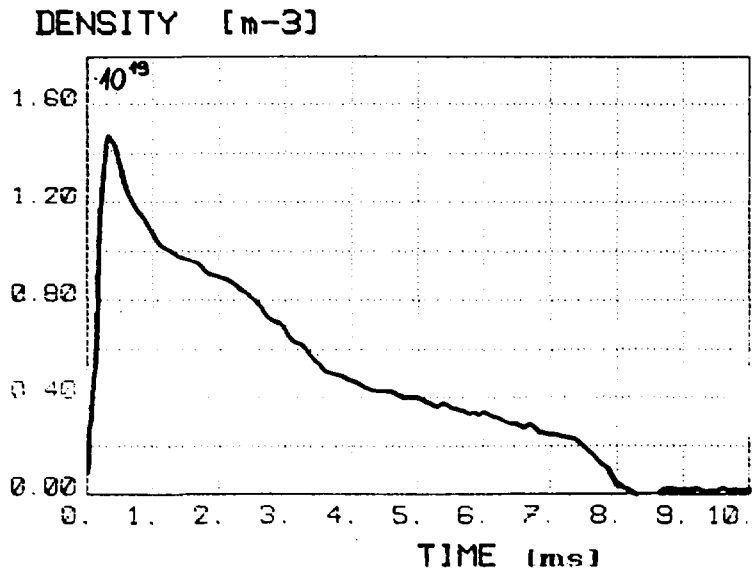
DENSITY [m-3]
10^19
1.60
1.20
0.80
0.40
0.00
0. 1. 2. 3. 4. 5. 6. 7. 8. 9. 10.
TIME [ms]

Fig. 12

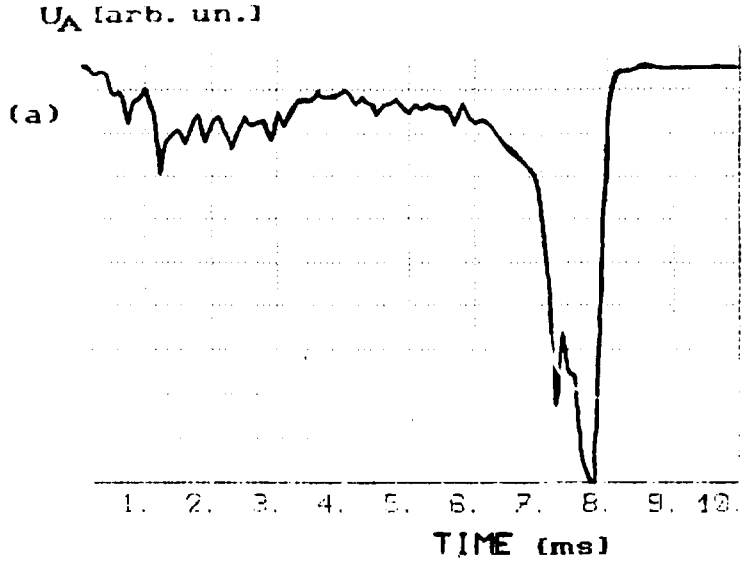
U_A [arb. un.]
(a)
1. 2. 3. 4. 5. 6. 7. 8. 9. 10.
TIME [ms]

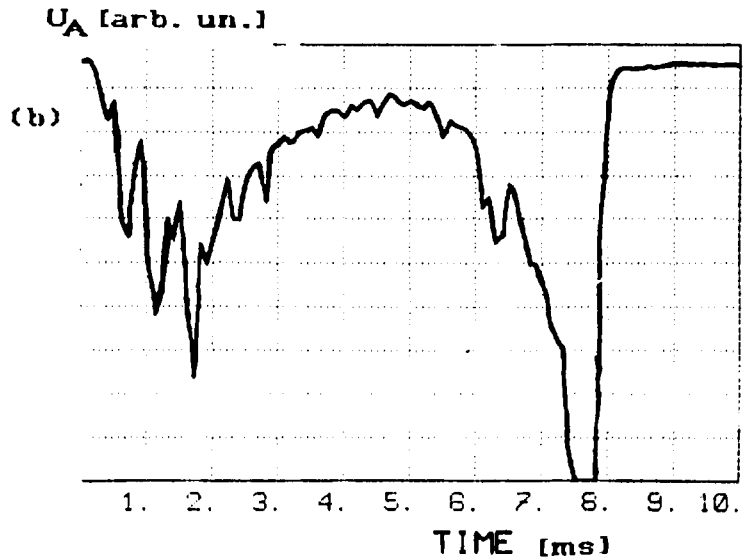
U_A [arb. un.]
(b)
1. 2. 3. 4. 5. 6. 7. 8. 9. 10.
TIME [ms]

Fig. 13

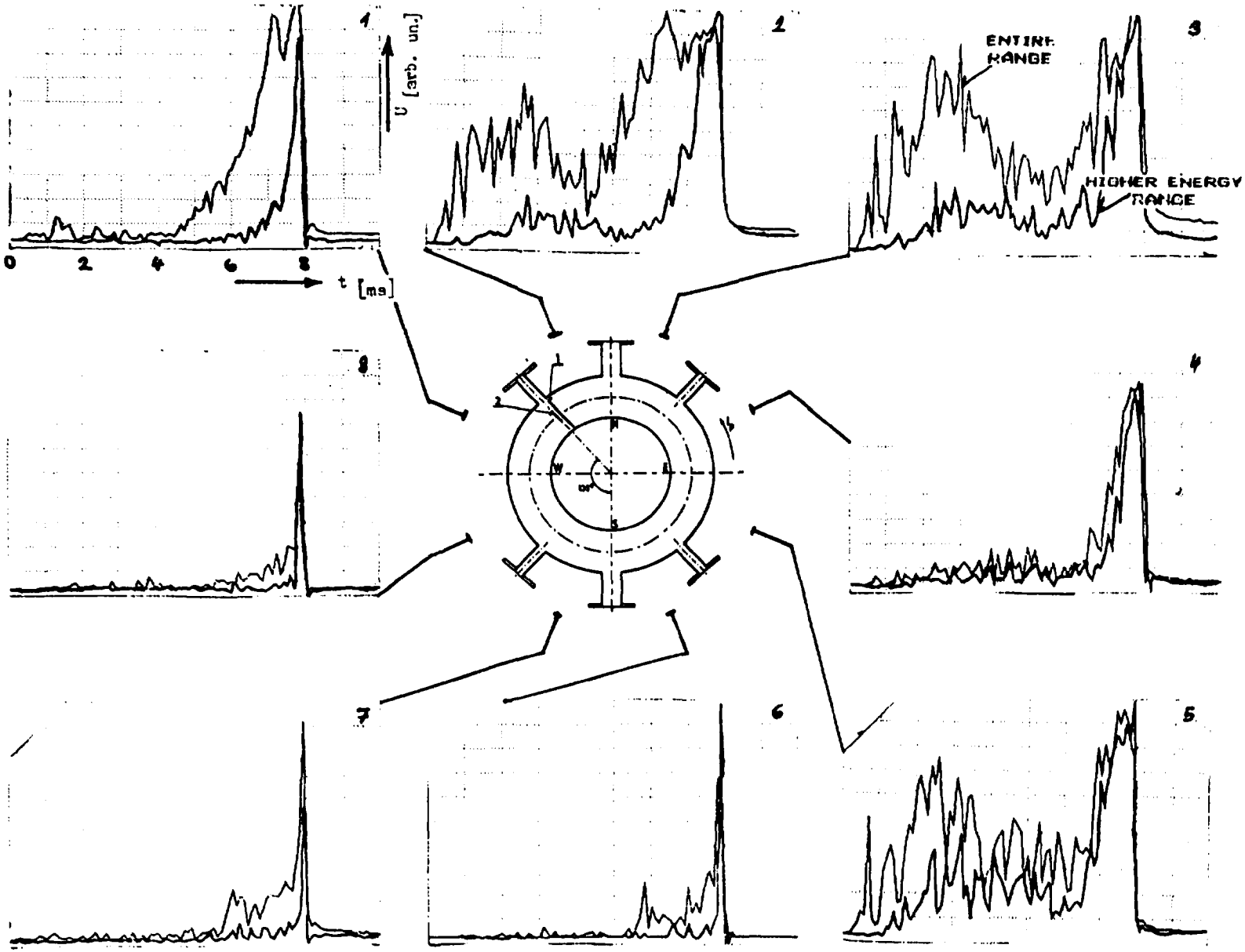
1
U [arb. un.]
0
2
4
6
8
t [ms]
2
3
ENTINF. RANGE
HIGHER ENERGY RANGE
8
4
7
6
5

Fig. 14

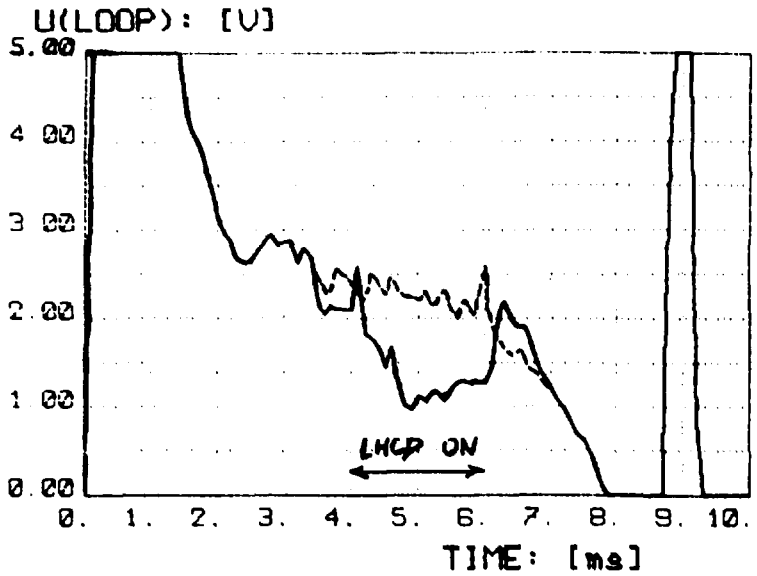
U(LOOP): [V]
5.00
4.00
3.00
2.00
1.00
0.00
LHCD ON
0. 1. 2. 3. 4. 5. 6. 7. 8. 9. 10.
TIME: [ms]

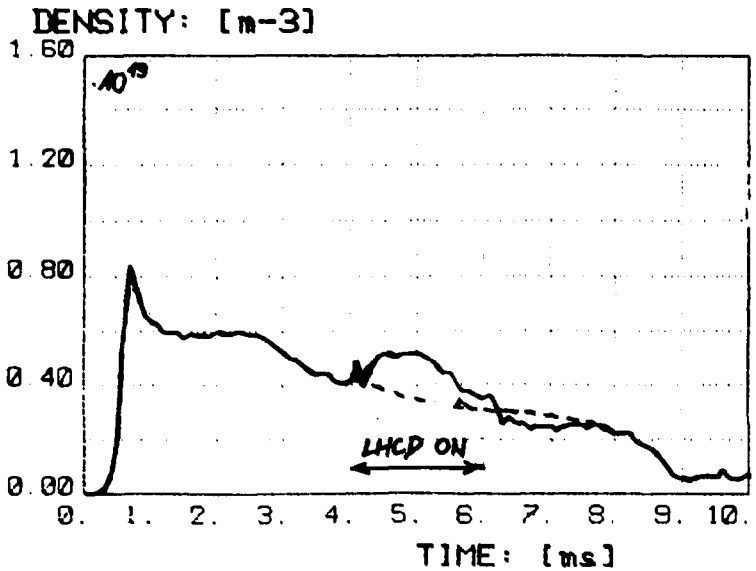
DENSITY: [m-3]
1.60
10^19
1.20
0.80
0.40
0.00
LHCD ON
0. 1. 2. 3. 4. 5. 6. 7. 8. 9. 10.
TIME: [ms]

Fig. 15

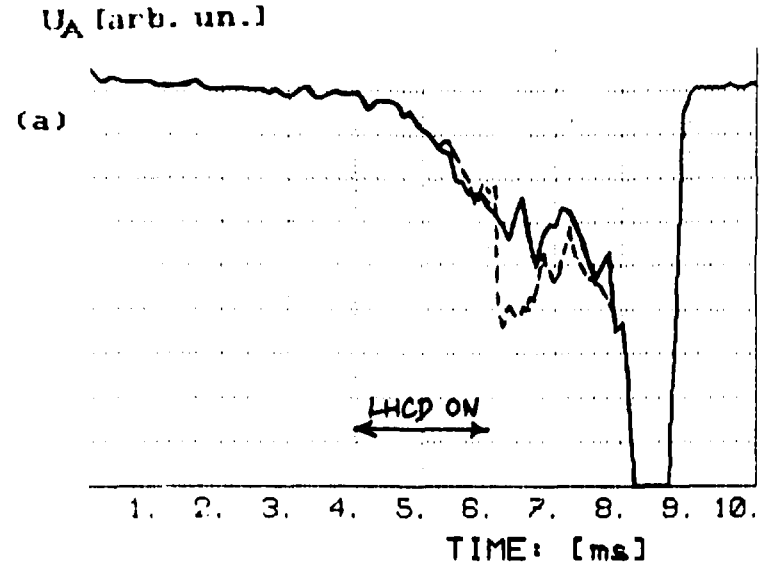
U_A [arb. un.]
(a)
LHCD ON
1. 2. 3. 4. 5. 6. 7. 8. 9. 10.
TIME: [ms]

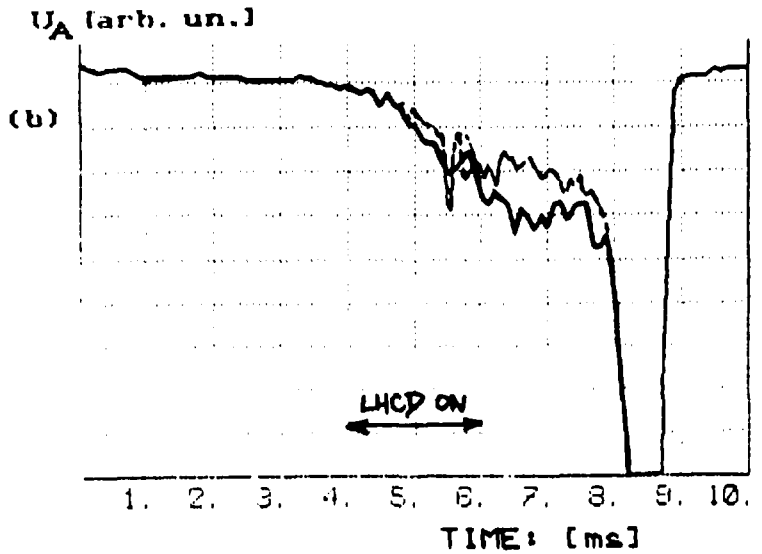
U_A [arb. un.]
(b)
LHCD ON
1. 2. 3. 4. 5. 6. 7. 8. 9. 10.
TIME: [ms]

Fig. 16

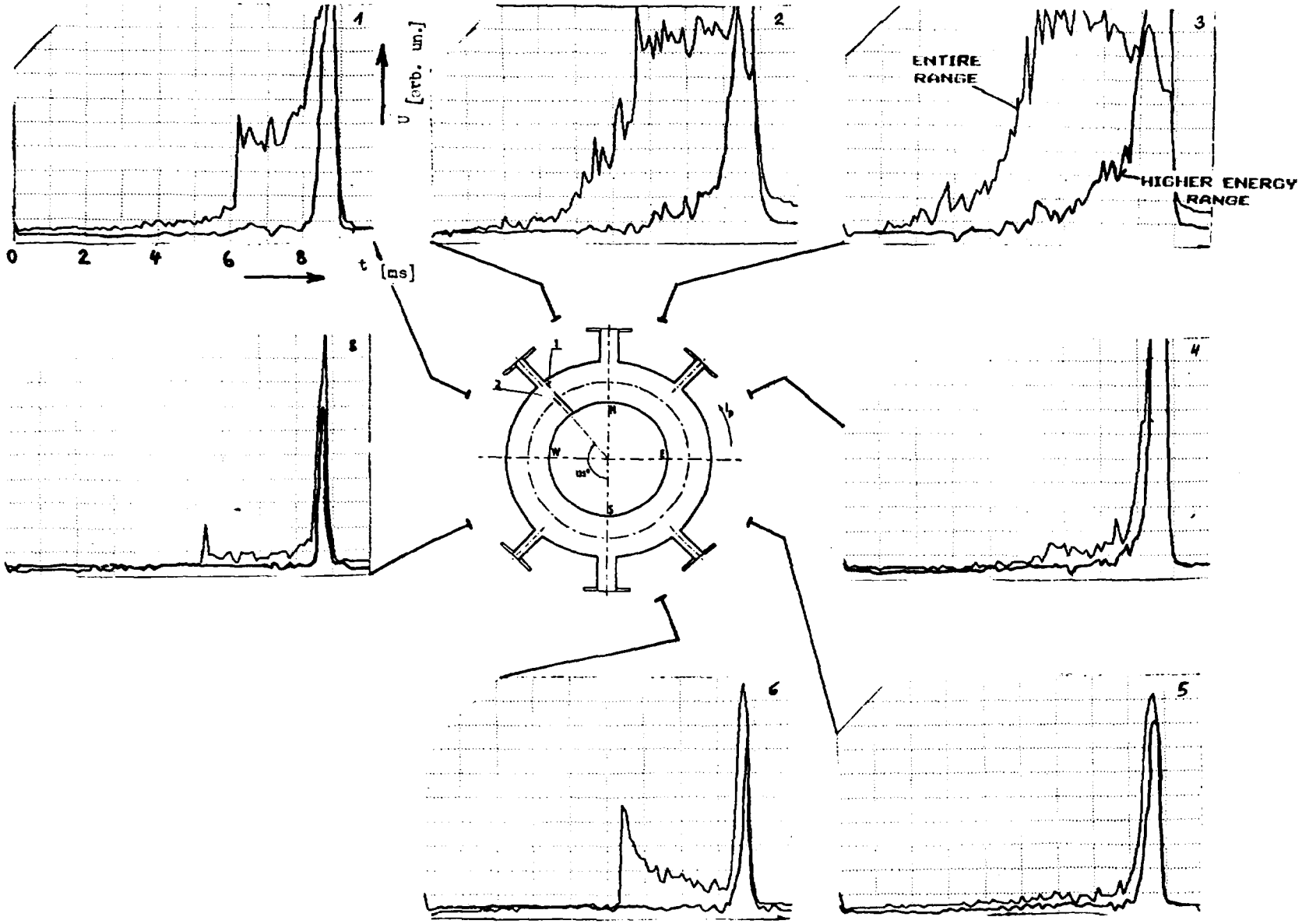

Fig. 17

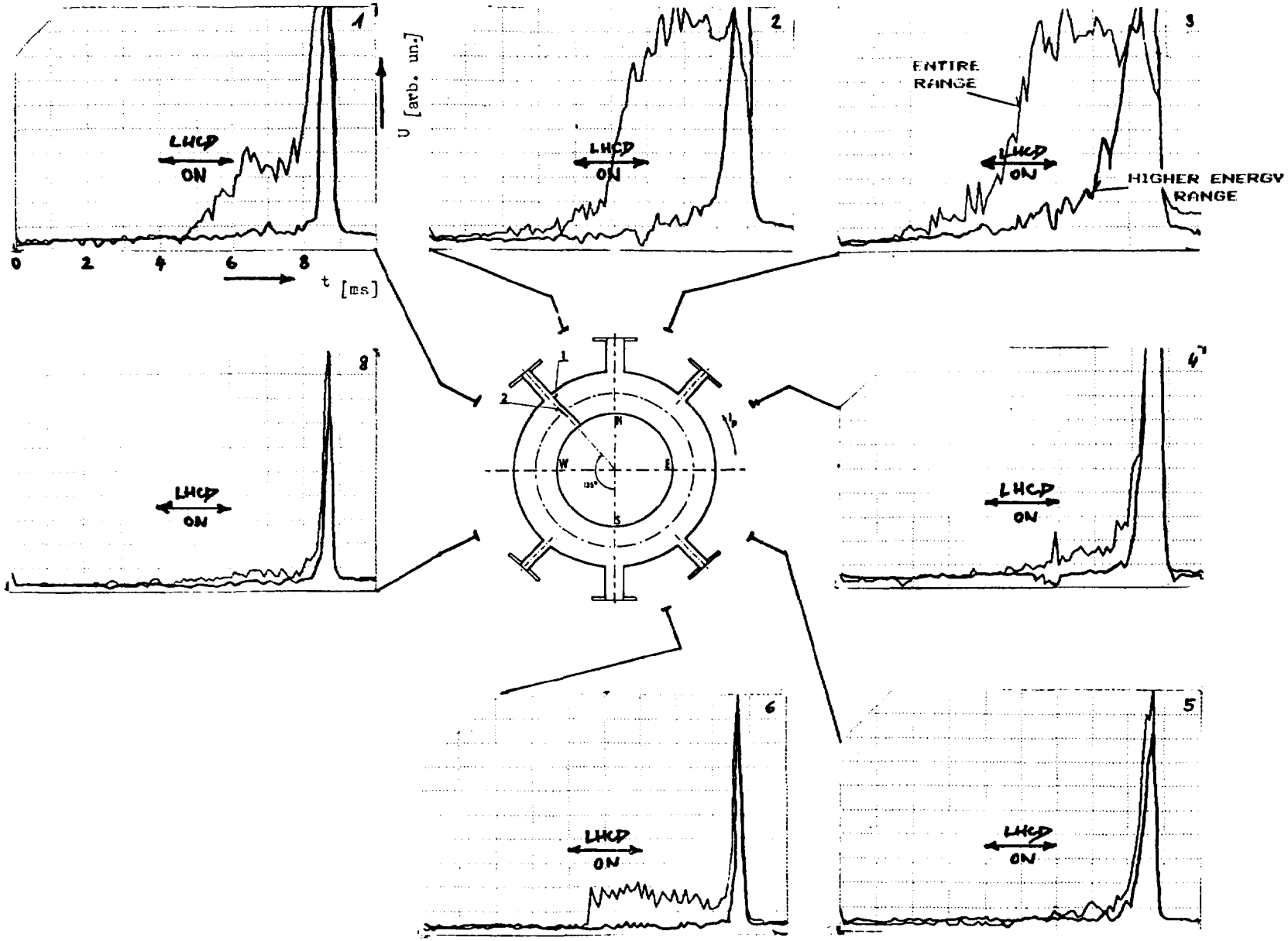
1
LHCD
ON
U [arb. un.]
0
2
4
6
8
t [ms]
2
LHCD
ON
3
ENTIRE
RANGE
LHCD
ON
HIGHER ENERGY
RANGE
8
LHCD
ON
1
2
N
W
E
S
4
LHCD
ON
6
LHCD
ON
5
LHCD
ON

Fig. 18

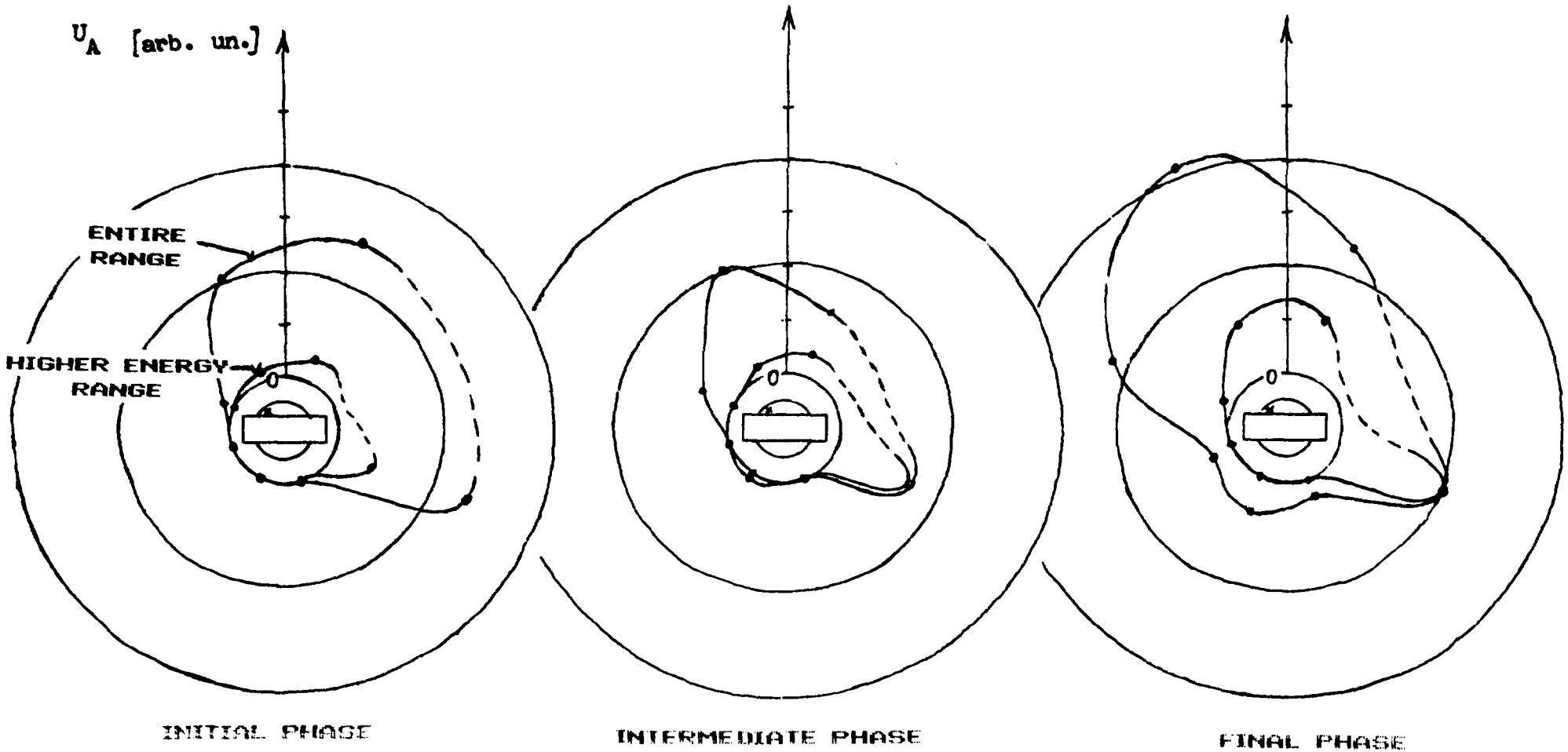
U_A [arb. un.]
ENTIRE RANGE
HIGHER ENERGY RANGE
0
0
0
INITIAL PHASE
INTERMEDIATE PHASE
FINAL PHASE

Fig. 19

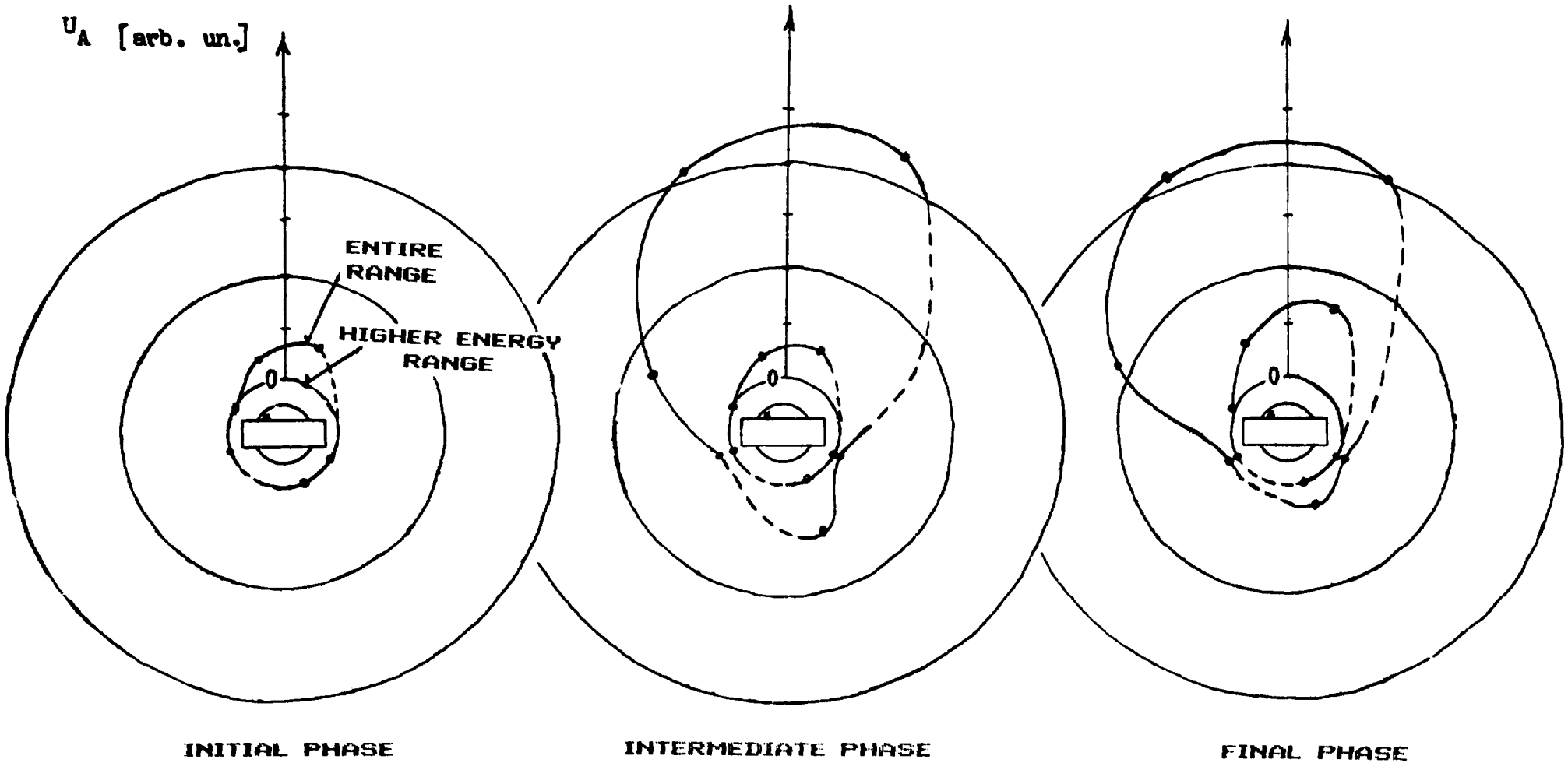
U_A [arb. un.]
ENTIRE RANGE
HIGHER ENERGY RANGE
0
0
0
INITIAL PHASE
INTERMEDIATE PHASE
FINAL PHASE

Fig. 20

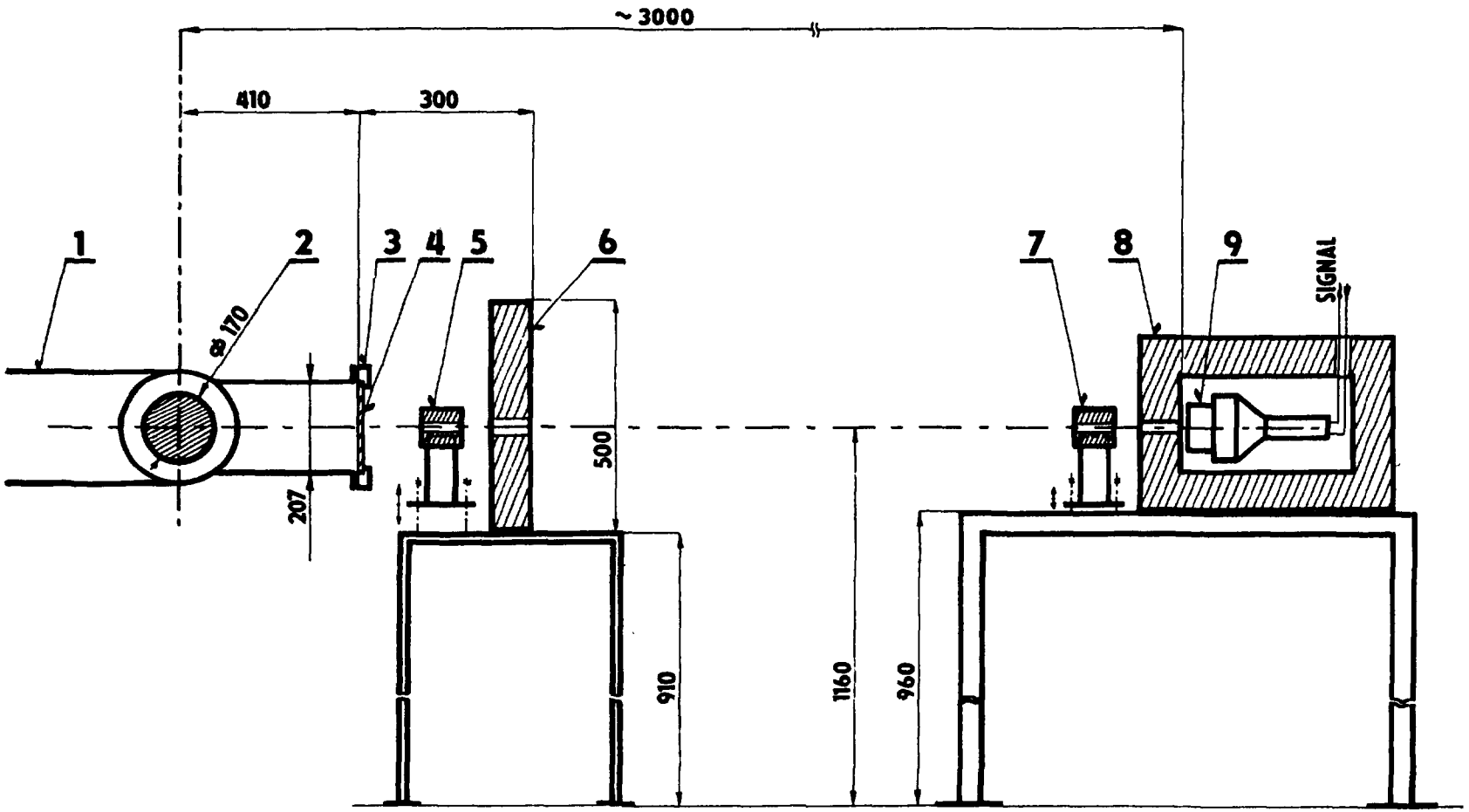

Fig. 21